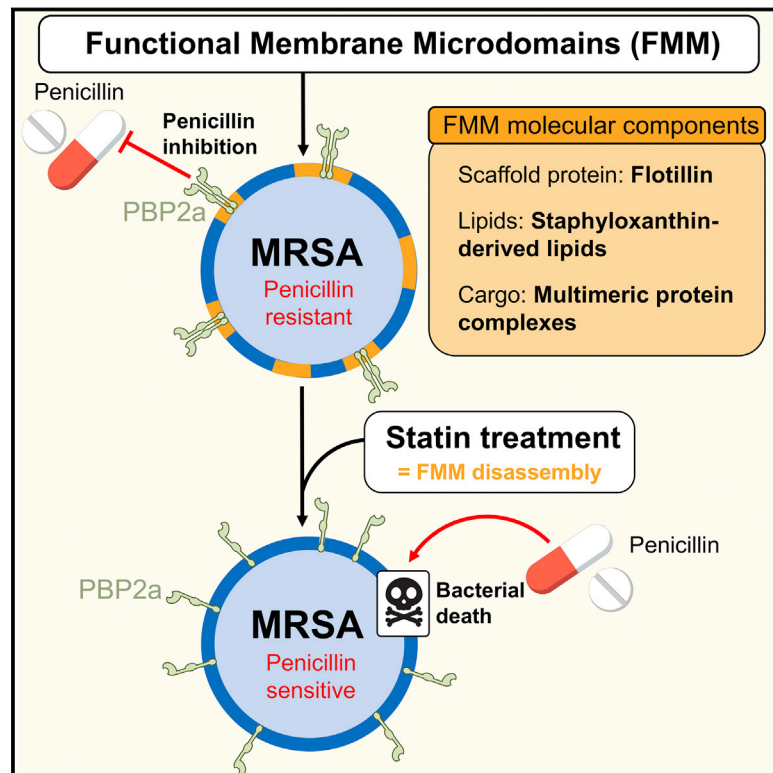


Membrane Microdomain Disassembly Inhibits MRSA Antibiotic Resistance

Graphical Abstract



Authors

Esther García-Fernández, Gudrun Koch, Rabea M. Wagner, ..., Sebastian M. Markert, Christian Stigloher, Daniel Lopez

Correspondence

dlopez@cnb.csic.es

In Brief

Using statins to disassemble bacterial membrane microdomains can decrease antibiotic resistance and re-sensitize MRSA to antibiotic therapies *in vivo*.

Highlights

- Staphyloxanthin and flotillin preferentially interact and accumulate in FMMs
- FMMs facilitate efficient oligomerization of multimeric protein complexes
- PBP2a, which confers β -lactam resistance on *S. aureus*, is harbored within FMMs
- FMM disruption disables PBP2a oligomerization and thus, *S. aureus* antibiotic resistance



Membrane Microdomain Disassembly Inhibits MRSA Antibiotic Resistance

Esther García-Fernández,^{1,7} Gudrun Koch,^{2,3,7} Rabea M. Wagner,^{1,2,3} Agnes Fekete,⁴ Stephanie T. Stengel,^{2,3} Johannes Schneider,^{2,3} Benjamin Mielich-Süss,^{2,3} Sebastian Geibel,^{2,3} Sebastian M. Markert,⁵ Christian Stigloher,⁵ and Daniel Lopez^{1,2,3,6,8,*}

¹National Centre for Biotechnology, Spanish National Research Council (CNB-CSIC), 28049 Madrid, Spain

²Research Centre for Infectious Diseases (ZINF), University of Würzburg, 97080 Würzburg, Germany

³Institute for Molecular Infection Biology (IMIB), University of Würzburg, 97080 Würzburg, Germany

⁴Julius-von-Sachs-Institute Biocenter, Pharmaceutical Biology, University of Würzburg, 97082 Würzburg, Germany

⁵Division of Electron Microscopy, Biocenter, University of Würzburg, 97074 Würzburg, Germany

⁶National Centre for Biotechnology, Spanish National Research Council (CNB-CSIC), Darwin 3, Campus de Cantoblanco, 28049 Madrid, Spain

⁷These authors contributed equally

⁸Lead Contact

*Correspondence: dlopez@cnb.csic.es

<https://doi.org/10.1016/j.cell.2017.10.012>

SUMMARY

A number of bacterial cell processes are confined functional membrane microdomains (FMMs), structurally and functionally similar to lipid rafts of eukaryotic cells. How bacteria organize these intricate platforms and what their biological significance is remain important questions. Using the pathogen methicillin-resistant *Staphylococcus aureus* (MRSA), we show here that membrane-carotenoid interaction with the scaffold protein flotillin leads to FMM formation, which can be visualized using super-resolution array tomography. These membrane platforms accumulate multimeric protein complexes, for which flotillin facilitates efficient oligomerization. One of these proteins is PBP2a, responsible for penicillin resistance in MRSA. Flotillin mutants are defective in PBP2a oligomerization. Perturbation of FMM assembly using available drugs interferes with PBP2a oligomerization and disables MRSA penicillin resistance *in vitro* and *in vivo*, resulting in MRSA infections that are susceptible to penicillin treatment. Our study demonstrates that bacteria possess sophisticated cell organization programs and defines alternative therapies to fight multidrug-resistant pathogens using conventional antibiotics.

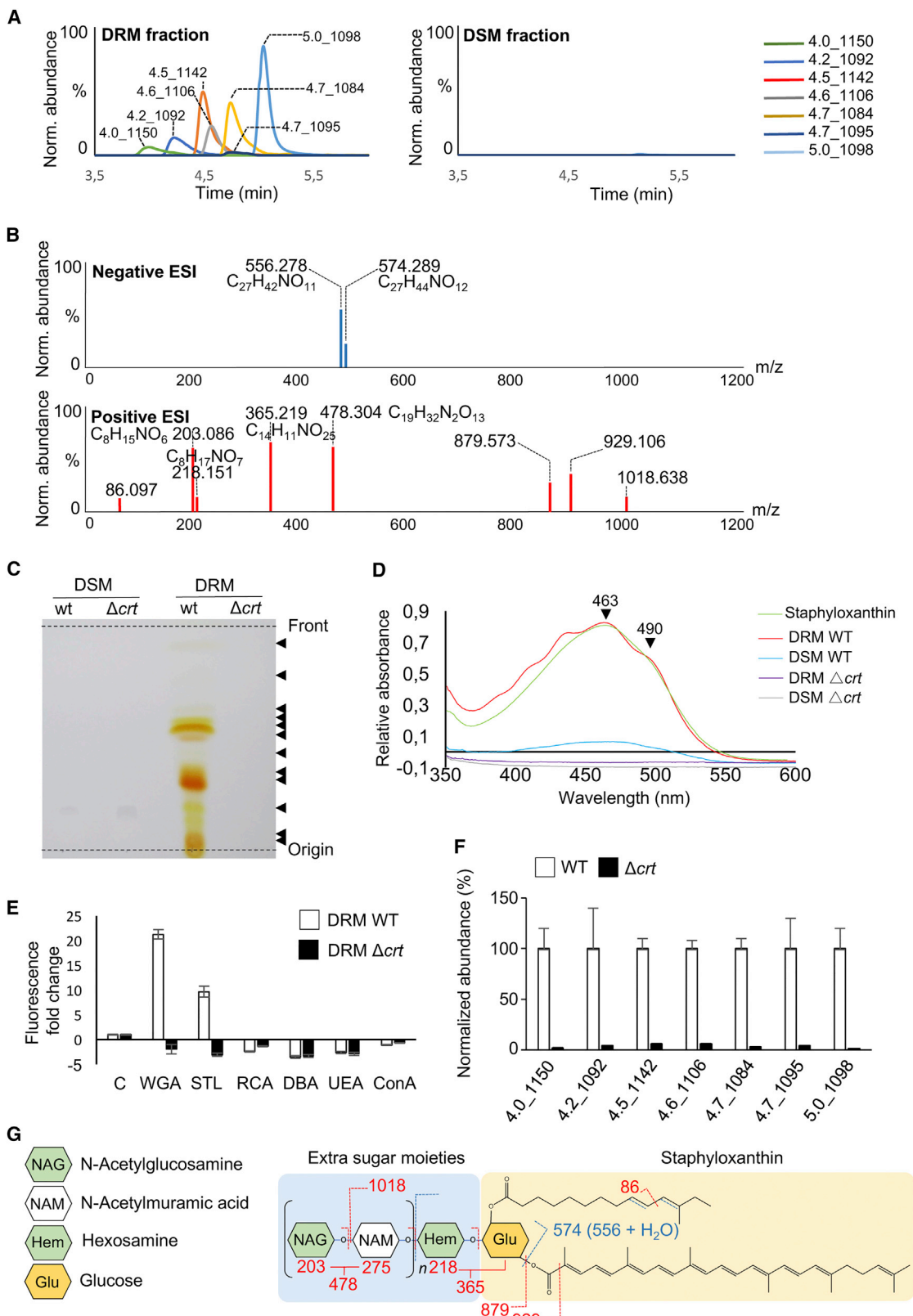
INTRODUCTION

Cell integrity depends on the correct organization of its limiting membrane, whose molecular organization we understand poorly. The pioneering fluid mosaic model suggested that membrane proteins and lipids diffuse freely and are thus homogeneously distributed (Singer and Nicolson, 1972), but recent advances show that membranes contain various lipid species

that segregate laterally into discrete microdomains (Kraft, 2013; Lorent and Levental, 2015). One of the most interesting examples in membrane organization is the formation of lipid rafts in eukaryotic cells. Eukaryotic cells organize proteins related to signal transduction and membrane trafficking into cholesterol- and sphingolipid-enriched membrane microdomains, or lipid rafts (Simons and Ikonen, 1997). Raft integrity requires the activity of the raft-associated scaffold protein flotillin, which recruits proteins to rafts to facilitate their interaction and oligomerization (Bickel et al., 1997). How cells organize lipid rafts is still unclear. Biochemical evidence nonetheless suggests that lipid rafts serve as platforms to control protein-protein interactions and to promote more efficient triggering of signal transduction cellular processes.

The existence of lipid rafts has been traditionally associated with eukaryotic cells; thus, raft assembly in eukaryotes has been considered a fundamental step during the evolution of cellular complexity, suggesting that prokaryotes do not require such sophisticated compartmentalization of their cellular processes. However, prokaryotic membranes compartmentalize diverse cell processes in raft-like regions termed functional membrane microdomains (FMMs), similar to their eukaryotic counterparts (LaRocca et al., 2013; López and Kolter, 2010). FMM formation in bacteria involves the biosynthesis and aggregation of still-unknown isoprenoid membrane lipids (Feng et al., 2014; López and Kolter, 2010) and their colocalization with flotillin homolog proteins (Donovan and Bramkamp, 2009; López and Kolter, 2010). Bacterial flotillins probably recruit protein cargo to FMMs to facilitate protein interaction and oligomerization (Bach and Bramkamp, 2013; Koch et al., 2017; Schneider et al., 2015), similar to eukaryotic flotillins. Flotillin-deficient strains have defects in biofilm formation in *Bacillus subtilis* and *Staphylococcus aureus* (Bach and Bramkamp, 2013; Koch et al., 2017; Schneider et al., 2015), virulence in *B. anthracis* (Somani et al., 2016) and *Campylobacter jejuni* (Heimesaat et al., 2014; Tareen et al., 2013), or thylakoid integrity in cyanobacteria (Bryan et al., 2011).

Despite this importance, the organization and biological significance of FMMs are largely unknown. Here, we addressed these



(legend on next page)

questions in the human pathogen *S. aureus*. In contrast to traditional bacterial models, *S. aureus* expresses a single flotillin, FloA, and the biosynthesis pathway for isoprenoid membrane lipids is fairly well known (Marshall and Wilmoth, 1981; Pelz et al., 2005; Wieland et al., 1994), rendering a realistic model in which to undertake FMM organizational and functional studies. In addition, *S. aureus* attracts considerable attention of the scientific community, as it causes hard-to-treat hospital-associated infections due to its capacity to overcome antibiotic treatments. *S. aureus* acquires resistance to β -lactam antibiotics such as methicillin (methicillin-resistant *S. aureus*; MRSA) (Kreiwirth et al., 1993) through expression of a low-affinity penicillin-binding protein (PBP2a) that acts cooperatively with the general penicillin-binding protein PBP2 (Fishovitz et al., 2014; Pinho et al., 2001a). β -lactam antibiotics bind the PBP active site as substrate analogs (Zapun et al., 2008) to inhibit the PBP activity responsible for peptidoglycan synthesis during cell division. The PBP2a active site is located in a deep pocket inaccessible to β -lactam antibiotics (Otero et al., 2013), licensing MRSA strains to divide and proliferate in their presence (Kreiwirth et al., 1993).

We show that FMM organization in MRSA requires lateral segregation of unphosphorylated carotenoids (staphyloxanthin and derivative lipids) in membrane microdomains. Flotillin preferentially binds to these lipids and oligomerizes in these domains, followed by attraction of membrane-associated multimeric complexes with which flotillin interacts and promotes efficient oligomerization. One of these proteins is PBP2a. Flotillin scaffold activity promotes PBP2a oligomerization; perturbation of FMM assembly using standard hypercholesterolemia drugs interferes with biosynthesis of FMM constituent lipids, which affects flotillin activity and ultimately, PBP2a oligomerization. This disables penicillin resistance in MRSA in a murine infection model, resulting in MRSA infections susceptible to penicillin antibiotic treatments. This study shows that bacterial cells organize sophisticated programs for membrane compartmentalization and defines an innovative strategy to overcome MRSA antibiotic resistance and help reduce the high mortality rates caused by invasive MRSA infections.

RESULTS

Constituent Lipids of FMMs Are Carotenoids

Organization of FMMs in bacteria relies on the scaffold protein flotillin and aggregation of isoprenoid lipids of yet unknown na-

ture (Bramkamp and Lopez, 2015). To identify the constituent lipids and the mechanism of FMM assembly, we purified *Staphylococcus aureus* MRSA strain USA300LAC (McDougal et al., 2003) cell membranes. Given the different lipid composition and density of FMMs, a FMM-rich sample can be obtained by exploiting the FMMs' insolubility after treatment with nonionic detergents (0.5%–1% Triton X-100, 4°C) prior to phase separation (Brown, 2002). This treatment generates a membrane fraction sensitive to detergent disaggregation (detergent-sensitive membrane; DSM) and another that is resistant to disruption with larger FMM-rich fragments (detergent-resistant membrane; DRM). Total lipids were extracted from DRM and DSM fractions and membrane lipids identified in untargeted lipidomics experiments using electrospray ionization (UPLC-ESI-qTOF-MS) (Figures S1A and S1B and Table S1). In all, 39 lipid species were unique in the DRM compared to the control sample (extraction solution with no cells). From the 39 peaks, intensities of 30 peaks were clearly higher in DRM than in DSM; 7 were detected consistently in 3 independent biological replicates ($n = 3$) and were thus considered FMM lipid markers (fold change > 100, Figure 1A and Table S1).

These seven FMM lipid markers were annotated according to retention times (RTs) and nominal mass-to-charge ratios (m/z) (Figure 1A). All marker ions were doubly charged, as the m/z difference of the isotope peaks were 0.50, and their low RT suggested polar characteristics (Figure S1C). Product ion scan at negative electrospray ionization ESI showed two common fragments of 556.28 and 574.29 m/z (Figure 1B), which denotes that these marker lipids belong to the same class. No fragments of glycerol-3-phosphate ion (152.99 m/z), $H_2PO_4^-$ ion (96.97 m/z) or PO_3^- ion (78.96 m/z) were detected in the mass spectrometry (MS)/MS spectra, indicating that these are not membrane phospholipids. Elemental composition of these two peaks ($C_{27}H_{44}NO_{12}$ and $C_{27}H_{42}NO_{11}$, the same molecule with and without one H_2O) is consistent with that of a staphyloxanthin fragment in which the sugar backbone is decorated with an extra sugar. Product ion scan at positive ESI detected neutral losses of N-acetylglucosamine alone (NAG; 203.09) and with N-acetylmuramic acid (NAG-NAM; 478.30), thus categorizing FMM markers as staphyloxanthin-derived unphosphorylated saccharolipids in which fatty acids are linked directly to a NAM-NAG-containing sugar backbone.

Staphyloxanthin is an unphosphorylated saccharolipid of isoprenoid nature found in *S. aureus* membranes that gives

Figure 1. Identification of FMM-Constituent Lipids

(A) Ion chromatogram of FMM lipid markers in DRM (left) and DSM (right) fractions, labeled with RT and m/z ratios. Lipid abundance represented in absorbance units.

(B) Fragmentation pattern of FMM lipid markers at negative (top) and positive (bottom) ESI by product ion scan (MS/MS). Common fragments with respective MW and tentative formulas are shown.

(C) (Top) TLC detection of staphyloxanthin lipids in DRM and DSM fractions of WT and Δcrt mutant. Staphyloxanthin lipids are visualized as yellow-pigmented bands (arrowheads).

(D) UV-visible spectroscopy of purified staphyloxanthin and DRM and DSM samples (WT and Δcrt mutant). Arrowheads indicate characteristic 463- and 490-nm staphyloxanthin peaks.

(E) Fluorescein-labeled lectin binding assay to WT and Δcrt DRM samples. WGA, wheat germ agglutinin; STL, *Solanum tuberosum* lectin; RCA, *Ricinus communis* agglutinin; DBA, *Dolichos biflorus* agglutinin; UEA, *Ulex europaeus* agglutinin; ConA, concanavalin A.

(F) Relative abundance of FMM lipid markers in WT and Δcrt mutant using ion chromatography. Data shown as mean \pm SD for three biological replicates ($n = 3$).

(G) Tentative molecular structure and fragmentation pattern (blue, negative ESI; red, positive ESI) of staphyloxanthin-related FMM lipid markers.

See also Figures S1 and S2 and Tables S1 and S4.

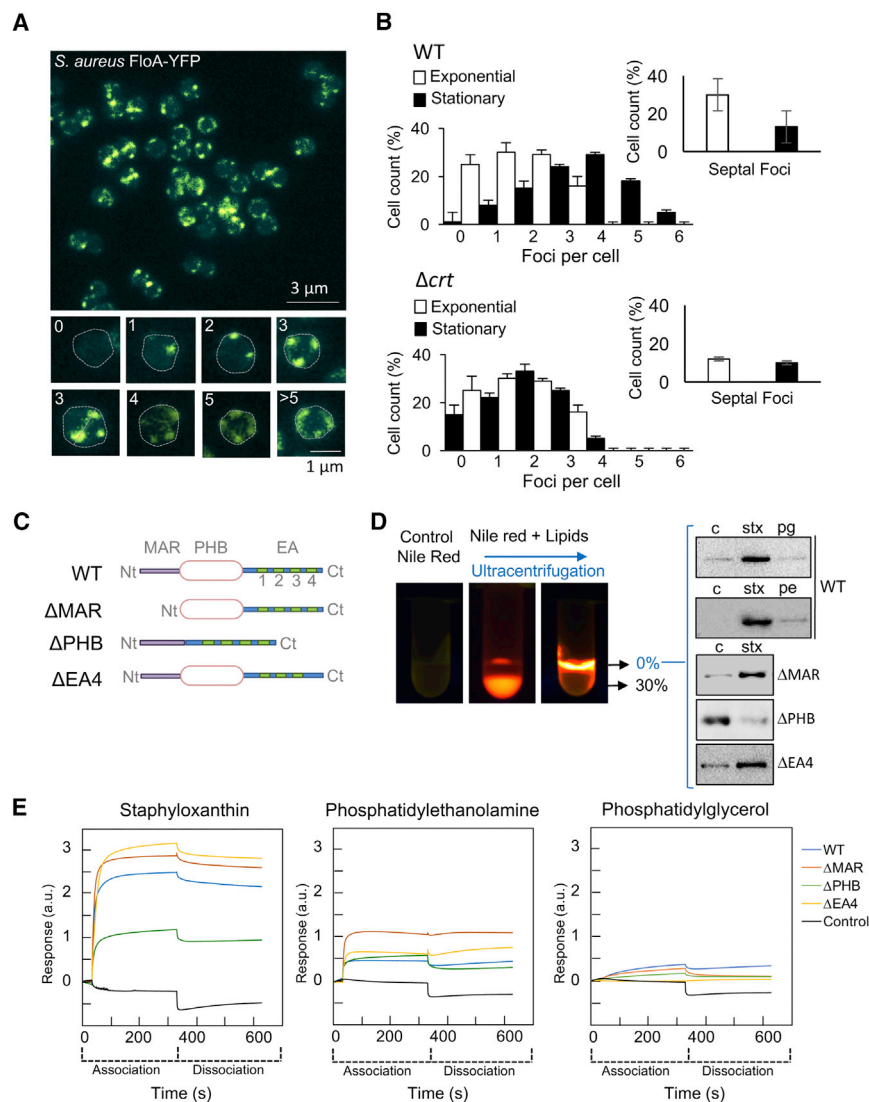


Figure 2. FMM-Constituent Lipids and Flo-tillin Preferentially Interact

(A) Fluorescence micrographs of MRSA cells expressing FloA-YFP. (Bottom) Detail of flotillin focus localization and cell numbers. Two images show three foci in a dividing and a non-dividing cell. Dividing cells show foci at septal invaginations.

(B) Quantification of focus number in WT and Δcrt mutant in exponential and stationary phase. (Insets) Quantification of septal focus number. We counted 700 random cells from each of 3 microscopic fields from independent experiments ($n = 2100$ cells per strain).

(C) Scheme of WT, ΔMAR , ΔPHB , and $\Delta EA4$ flotillin variants.

(D) Lipid-binding flotation assay. (Left) Flotation assay images using Nile red (NR) for lipid staining. NR is fluorescent only in the presence of lipids. After ultracentrifugation, lipids migrate to the low-density sucrose fraction (0% sucrose; tube top). (Right) FloA immunodetection in the lipid fraction (0% sucrose) after ultracentrifugation. C, control with no lipids; Stx, with staphyloxanthin lipids; pg, with phosphatidylglycerol (phospholipid).

(E) Lipid-protein interaction of staphyloxanthin and phosphatidylglycerol with flotillin variants determined using BLI. Negative control (black line) is a cytoplasmic lactonase (YtnP) that does not interact with lipids (Schneider et al., 2012). Data shown as mean for three biological replicates ($n = 3$). Response measured in arbitrary units (a.u.).

See also Figures S2 and S3 and Table S4.

Accumulation of Flotillin and Lipid Markers Drives FMM Assembly

Our current hypothesis states that FMM assembly requires lateral segregation of FMM lipids in specific microdomains together with recruitment of flotillin (FloA) to these regions. We used a translational fusion of flotillin to a yellow fluorescence protein (FloA-YFP) to detect FloA orga-

nized in discrete dynamic foci distributed across the cell membrane in exponentially growing and stationary cells (Figures 2A, 2B, and S2C). While WT stationary cells showed an average of five foci per cell, the Δcrt mutant showed fewer foci (two foci per cell). WT and Δcrt cultures in exponential growth showed reduced numbers of foci, as staphyloxanthin accumulates in cell membranes in the stationary phase (Kullik et al., 1998) (Figure S2D). Foci were distributed on the membrane in no specific pattern, although dividing cells generally showed foci near the invaginations of the division septum. A small number of septal foci was also detected in the Δcrt mutant (Figure 2B).

S. aureus its typical yellow color (Pelz et al., 2005). We used thin-layer chromatography (TLC) to identify staphyloxanthin-pigmented bands in the DRM sample; no pigmented bands were detected in the DSM sample of wild-type (WT) or samples from a *S. aureus* Δcrt mutant that lacks the operon for staphyloxanthin biosynthesis (Figure 1C). UV-visible spectroscopy of a FMM lipid sample showed peaks at 463 and 490 nm, typical of purified staphyloxanthin (Figure 1D), which indicated that FMM lipids are staphyloxanthin derivatives. In immunodetection assays using labeled lectins, only wheat germ lectin (WGA) and *Solanum tuberosum* lectin (STL) detected positive signals specific for NAG and NAG-NAM, respectively (Figures 1E and S2A). Using UPLC-ESI-qTOF-MS, we did not detect any of the seven FMM lipid markers in the Δcrt mutant DRM or DSM fractions (Figures 1F and S2B), which indicated that staphyloxanthin-derived NAG-NAM-decorated lipids are highly represented in the FMM. A tentative formula consistent with the fragmentation pattern is shown (Figure 1G).

To evaluate FloA recruitment to staphyloxanthin-rich microdomains, we quantified staphyloxanthin-FloA interaction using lipid-protein flotation and binding assays with distinct FloA variants (Figure 2C). In the flotation assay, FloA and lipids were mixed beneath a sucrose gradient. After ultracentrifugation, lipids migrated to the low-sucrose-density fraction at the top of the tube accompanied by FloA only when interaction occurred,

as detected with FloA-specific antibodies (Figure 2D). Purified WT FloA interacted strongly with purified staphyloxanthin, but not with phospholipids (phosphatidylglycerol, PG; phosphatidylethanolamine, PE). A Δ MAR variant that lacks the N-terminal membrane-anchoring region also interacted strongly with purified staphyloxanthin, as did a Δ EA4 variant altered in one of its four C-terminal glutamine-alanine (EA) repeats, which probably participate in protein-protein interaction (Schneider et al., 2015). A Δ PHB variant lacking the prohibitin domain (PHB), whose function is unknown and is found in all flotillin-related proteins (Bach and Bramkamp, 2015), showed no tendency to interact with staphyloxanthin.

In the binding assay, purified staphyloxanthin was immobilized on a biosensor tip, followed by bio-layer interferometry (BLI). As FloA variants bind to the lipids with different affinity, incident light directed through the biosensor shifts and creates a quantifiable interference pattern (Figures 2E, S3A, and S3B). WT, Δ MAR, and Δ EA4 showed preferential affinity for staphyloxanthin compared to distinct membrane phospholipids ($K_D = 3.49 \times 10^{-8}$, 1.20×10^{-8} and 9.43×10^{-9} M, respectively), thus showing that FloA preferentially binds FMM-constituent lipids. In contrast, the Δ PHB variant showed no preference for staphyloxanthin over membrane phospholipids ($K_D = 9.43 \times 10^{-7}$ M). The flotillin PHB domain is thus responsible for the preferential interaction of flotillin with FMM-constituent lipids. Consequently, a YFP-labeled Δ PHB variant did not form membrane foci but was distributed homogeneously over the *S. aureus* membrane (Figure S3C).

FloA recognition of FMM lipids and confinement in microdomains could promote FloA-FloA interaction and, thus, FloA oligomerization in FMMs. FloA oligomeric states were resolved by size-exclusion chromatography (Figure 3A); we detected distinct peaks in the WT, Δ MAR, and Δ PHB profiles that were attributable to different oligomeric states, ranging from a 35 kDa monomer to a > 600 kDa oligomer. In contrast, the Δ EA4 profile showed no peaks corresponding to large oligomers, which indicated the importance of the C-terminal region in FloA multimerization. A YFP-labeled version of the Δ EA4 variant did not organize in membrane foci but showed homogeneous distribution over the *S. aureus* membrane (Figure S3C). Based on these results, we hypothesized that preferential staphyloxanthin-FloA binding via the PHB domain leads to FloA localization in staphyloxanthin-rich microdomains. The PHB domain is not involved in FloA oligomerization. FloA oligomerizes via a C-terminal interaction to organize FMMs (Figure 3B). To test this, we incubated purified FloA with purified staphyloxanthin- or phospholipid-containing suspensions and examined FloA oligomerization using electron microscopy (Figures 3C and S4A). We detected large FloA assemblies only in the staphyloxanthin-containing sample. Control samples with staphyloxanthin or phospholipids alone did not form large assemblies in our assay conditions. Using *in vivo* approaches, we monitored FloA oligomerization efficiency in *S. aureus*-purified membrane fractions of WT and Δ crt strains using blue-native (BN)-PAGE, which allows separation of membrane protein complexes in their natural oligomeric states (Wittig et al., 2006), or sucrose gradient centrifugation (5%–40%), and we detected FloA by immunoblotting (using an anti-FloA antibody) (Figure 3C). BN-PAGE showed a reduction in FloA-con-

taining high-molecular-weight (MW) protein complexes in Δ crt samples. In the sucrose gradient, the FloA signal concentrated in the high-density fractions, where high-MW protein complexes accumulated. In Δ crt, the FloA signal was detected in low-density fractions at the top of the tube, in which low-MW protein complexes accumulated. These results are consistent with the hypothesis that FMM assembly is a two-step process in which flotillin is recruited to staphyloxanthin-rich membrane microdomains, where it oligomerizes to organize FMMs.

Visualization of FMMs in Cell Membranes

Using super-resolution array tomography (srAT) (Markert et al., 2016) to visualize FMM assemblies in cell membranes, FloA was immunodetected and coarsely located in 100-nm sectioned cells using structured illumination microscopy (SIM) (Figures 4A and S4B). Next, samples were carbon-coated and imaged using scanning electron microscopy (Scan-EM). Fluorescence and Scan-EM images were correlated and FloA distribution was reconstructed. Flotillin was distributed in approximately five foci on the cell membrane, with no defined distribution pattern except its usual localization at septal invaginations in dividing cells. FloA-localizing regions were further examined by transmission electron microscopy (TEM). Uranyl acetate is typically used for section staining, as this stain binds preferentially to phospholipid phosphate head groups and provides intense contrast to membranes (Hayat, 1993; Ting-Beall, 1980). Our flotillin-containing microdomains nonetheless showed poor contrast and appeared as light electron-dense regions compared to the remainder of the membrane (Figure 4B). This is consistent with enrichment of unphosphorylated staphyloxanthin lipids in the FMM, which causes only light uranyl acetate staining of these microdomains, and with the lack of these light electron-dense regions in the Δ crt mutant (Figure S4C). We confirmed this observation using TEM, in which we simultaneously detected colocalization of FloA using immunogold labeling, and light electron-dense membrane regions using uranyl acetate staining, in 40- to 200-nm membrane microdomains (Figures 4C, 4D, and S4D). This finding indicates the possibility of visualizing FMMs using this approach.

Using super-resolution imaging by direct stochastic optical reconstruction microscopy (dSTORM), we examined subcellular flotillin location (Figure 5A). In *S. aureus* cells labeled with a SNAP-tagged FloA, switching of the fluorophore SNAP conjugate tetramethylrhodamine (TMR)-Star was used to reconstruct high-resolution images. As before, we found FloA located in membrane foci and near the septal invaginations of dividing cells. Approximately 25% of the FloA signal was detected in the cytoplasm surrounding the membrane foci, which suggested dynamic flotillin activity in these microdomains. Electron tomography was used to examine FloA-containing microdomains in greater detail (Figures 5B–5D and Movies S1, S2, and S3). Cells were uranyl-acetate-stained prior to performing the tilt series used to calculate 3D-image tomograms. FloA-localizing regions were identified in the tomograms as 100- to 300-nm light electron-dense membrane areas that stained poorly with uranyl acetate and showed accumulation of several nanodomains rather than a single uniform microdomain. The cytoplasmic area surrounding these membrane regions concentrated electron-dense

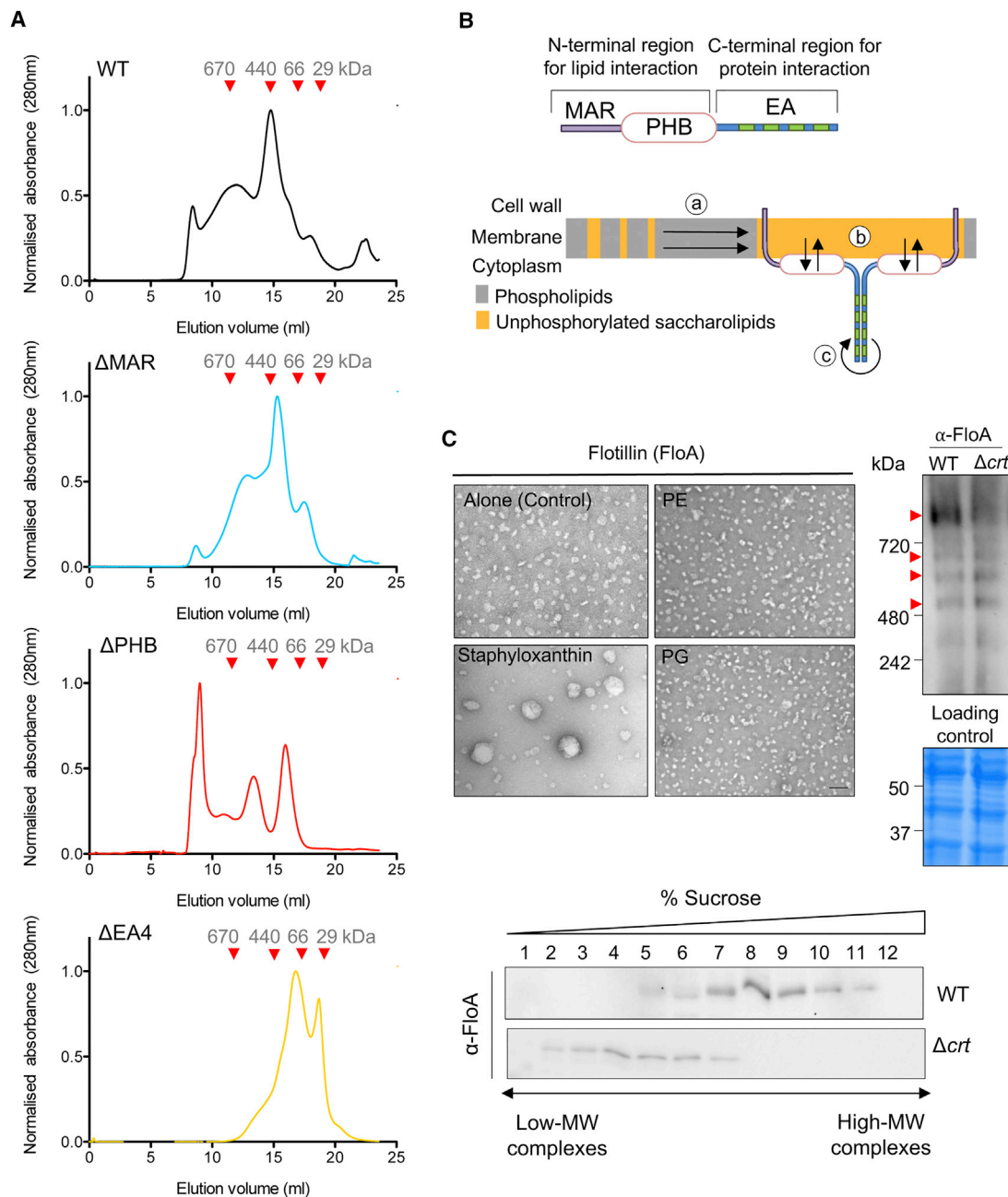


Figure 3. FMM-Constituent Lipids Promote Flotillin Oligomerization

(A) Size-exclusion chromatography profiles of WT, Δ MAR, Δ PHB, and Δ EA4 flotillin variants. Arrows show protein standards for calibration.

(B) Scheme of the molecular process that organizes bacterial FMM. (Top) Flotillin N-terminal region preferentially binds FMM-constituent lipids via PHB domain interaction, whereas the C-terminal region is responsible for flotillin oligomerization. (Bottom) (a) Constituent lipids aggregate in membrane microdomains based on similar physicochemical properties. (b) Flotillin is confined to these microdomains via staphyloxanthin-PHB interaction. (c) Flotillin oligomerizes via C-terminal interaction and accumulates to assemble FMM.

(C) (Left) TEM micrographs of purified flotillin oligomers alone or preincubated with staphyloxanthin, phosphatidylethanolamine (PE), or phosphatidylglycerol (PG). Staphyloxanthin-incubated oligomers generated larger protein assemblies. Scale bar, 50 nm. (Right) BN-PAGE and immunoblot to detect FloA oligomers in WT and Δ crt mutant and SDS-PAGE of the same samples as a loading control. (Lower panel) Immunoblot to detect FloA in the membrane fraction of WT (top) and Δ crt (bottom) strains resolved on a 5%–40% sucrose gradient (fractions 1–12).

See also Figure S4 and Table S4.

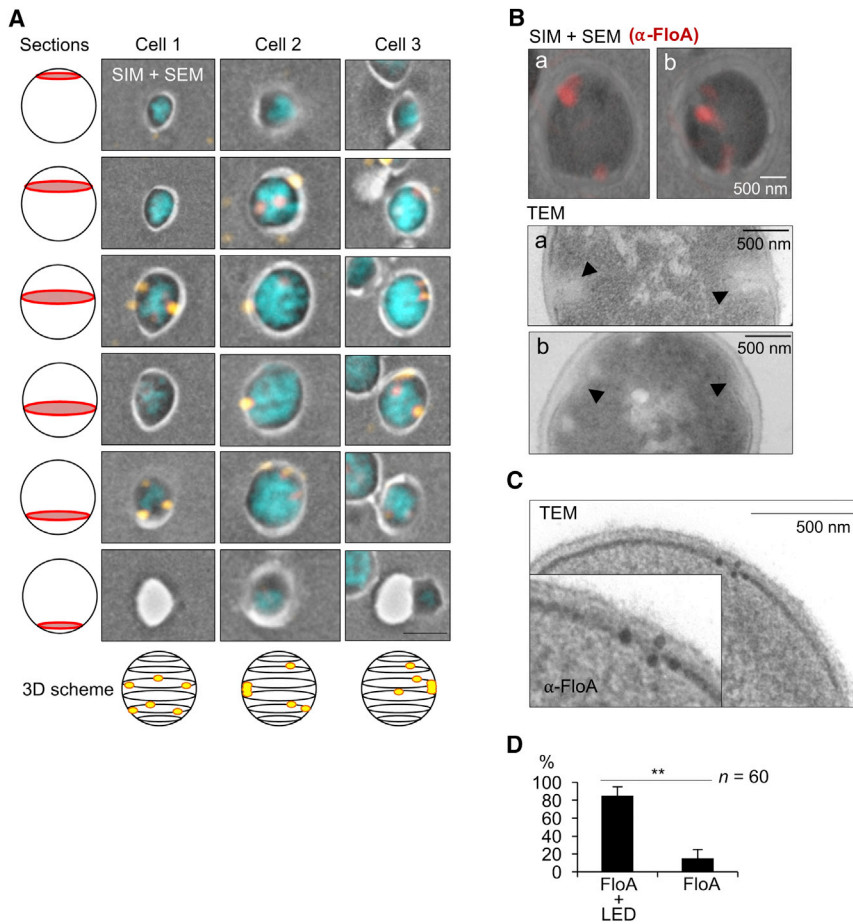


Figure 4. FMM Organization in *S. aureus* Membranes

(A) FloA immunodetection by whole-cell srAT (SIM + Scan-Em) micrographs of 100-nm sections of MRSA cells. Each column shows all sections of a given cell. Yellow indicates FloA immunodetection, blue indicates Hoechst-stained micrograph. A 3D reconstruction of FloA signal organization is shown beneath each column. Scale bar, 1 μ m.

(B) (Upper panel) FloA immunodetection in 100-nm sections of dividing cells, overlaid on a Scan-EM micrograph. FloA localizes near septal invaginations (a and b, in red). (Lower panel) TEM micrographs of septal invaginations to which FloA localizes (a and b, top), showing light electron-dense membrane regions (arrowheads). Scale bar, 500 nm.

(C) TEM micrographs showing immunogold detection of FloA in light electron-dense membrane areas. (Inset) Zoom of colocalizing region. Scale bar, 500 nm.

(D) Statistical analysis of FloA signal colocalization with light electron-dense membrane areas (LED) for 20 random cells from 3 independent experiments ($n = 60$). Data shown as mean \pm SD. Significance was measured using an unpaired Student's *t* test, ** $p < 0.01$.

See also [Figure S4](#), [Table S4](#), and [Movies S1](#), [S2](#), and [S3](#).

small particles, previously characterized as large protein complexes (McQuillen, 1962; Palade, 1955). We did not detect concentration of these particles in Δ *floA* tomograms (Movie S2), which suggested that FMMs engage in active protein organization, metabolism, and/or trafficking.

PBP2a Is Part of the FMM Protein Cargo

Having determined that FMMs could be involved in protein organization, we identified and quantified FMM-associated proteins by MS-based label-free quantification (LFQ) of total membrane proteome, DRM, and DSM fractions in distinct growth conditions (exponential [EXP], stationary [EST], late-stationary [LST], and nutrient-limiting [NLC]) (Figure 6A). Protein in DRM and DSM fractions was calculated relative to total membrane proteome content (\log_2 ratio), plotted for each condition tested, and shown in a heatmap using unsupervised hierarchical clustering (Figures 6B, S5, and Table S2). In DRM fractions, a core of \sim 100 proteins was consistently enriched in all conditions (Figure 6B; protein clusters A and B), whereas a number of other proteins were detected in these fractions in specific growth conditions (Figure 6B; protein clusters C [EXP], D [NLC], E [EST], and F [LST]). As control, detergent-extracted *n*-docecyl β -D-maltoside (DDM, 0.5%) DRM proteins were identified in a MS-based FloA pull-down assay (Table S3), which suggests that DRM proteins interact

with FloA and are thus FMM associated. Functional classification of FMM-associated proteins varies among the growth conditions (Figure 6C), although a common feature of all is their multimeric nature. We detected protein complexes

involved in membrane lipid metabolism (e.g., *mgt*, *lgt*, *MurJ*, *LtaA*, *UppP*, *TagH*, and *DitD*), membrane transport (*BmrA*, *Opp*, *CzcD*, *NarT*, *SirA*), protein quality control (*Sec*, *YajC*, *FtsH*), and virulence (*Rny*, *ebpS*, *T7SS*, *TcaA*), as well as proteins related to cell wall organization, such as *PBP2a* and others that can influence *PBP2a* activity, such as *PrsA*, *RodA*, or *PBP2* (Cho et al., 2016; Jousselin et al., 2012, 2015; Łeski and Tomasz, 2005; Pinho et al., 2001b).

Association of protein complexes with FMMs is consistent with their resemblance to eukaryotic lipid rafts and the role of rafts as platforms that promote efficient oligomerization between interacting protein partners. To explore this, we studied *PBP2a* as a case in point, given its importance in MRSA antimicrobial resistance. Furthermore, recent publications show *S. aureus* *PBP* localization in membrane foci in addition to their typical septal localization (Gautam et al., 2015; Monteiro et al., 2015). Physical interaction between *PBP2a* and FloA was detected first by heterologous *PBP2a* and FloA expression in a bacterial two-hybrid (B2H) assay (Figure 7A). Second, using pull-down experiments, we detected *PBP2a* in FloA co-eluted protein samples in immunoblot with anti-*PBP2a* antibodies (Figure 7B). Finally, srAT thin sections (100 nm) showed *PBP2a* transient colocalization with FloA in membrane foci (Figures 7C and S6A).

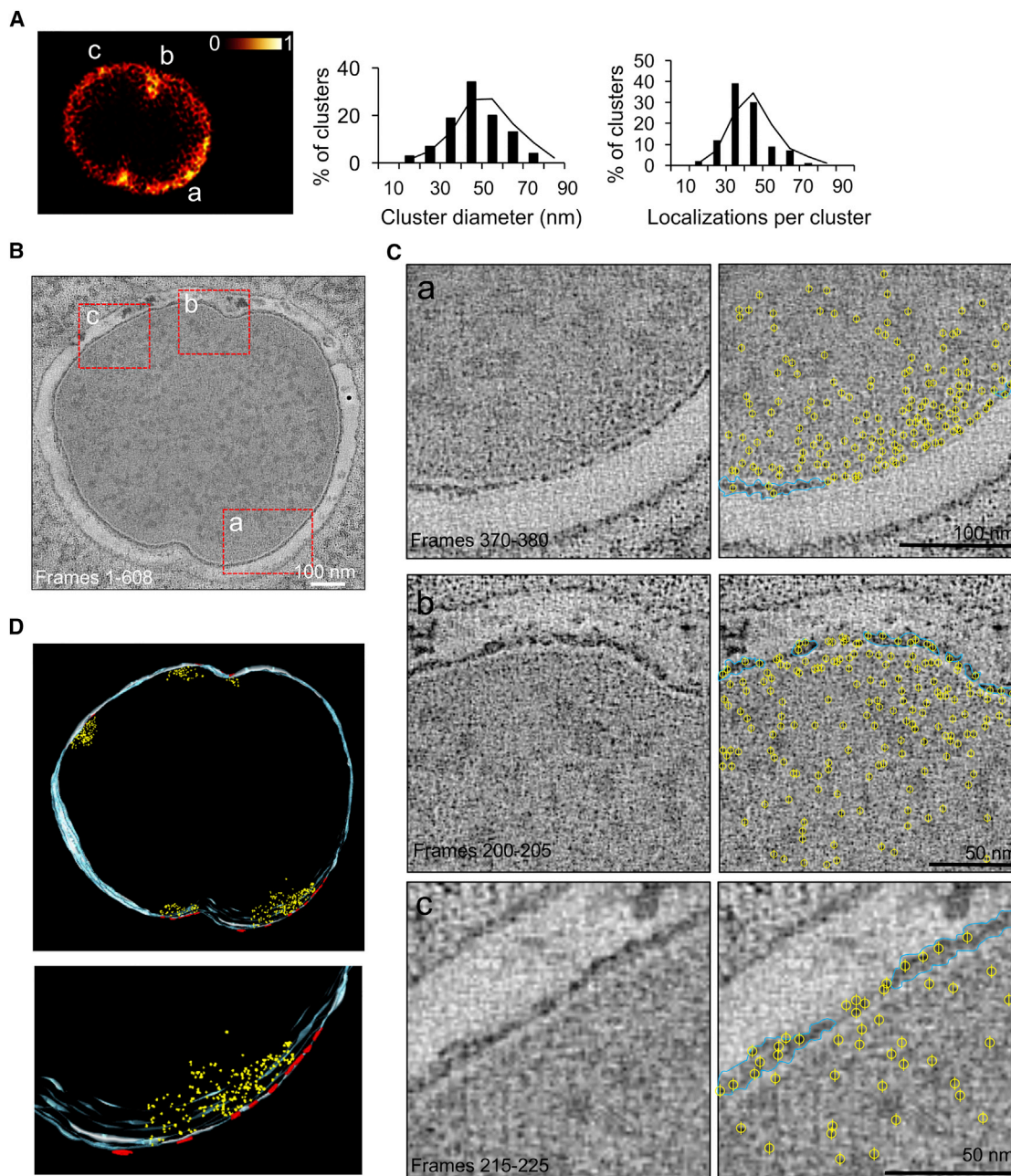


Figure 5. FMM Organization in *S. aureus* Membranes

(A) (Left) Flotillin localization analyzed by super-resolution microscopy. *d*STORM of *S. aureus* cells labeled with FloA-SNAP. Signal is detected in membrane foci (a, b, and c) and in surrounding cytoplasm. (Center, right) Mean flotillin cluster diameter and localizations per cluster for 20 random cells from 3 independent experiments ($n = 60$).

(B) Virtual slice of an electron tomogram of a *S. aureus* cell showing FloA localization (a, b, and c). Whole-cell view in [Movies S1](#) (WT) and [S2](#) (Δ *floA*).

(C) Magnified details of a, b, and c, showing light electron-dense membrane areas. Small electron-dense particles show higher concentration in surrounding cytoplasm. Segmentation of cell structures shows dark electron-dense membrane areas (blue contour) and small electron-dense particles (yellow). Each yellow contour denotes four adjacent black pixels.

(D) (Top) 3D model of the tomogram in (B), with (bottom) a detailed view of region a. [Movie S3](#) shows a 360° view of the model. Dark electron-dense membrane regions are shown in blue, light electron-dense nanodomains in red, and small electron-dense particles in yellow.

See also [Tables S2](#), [S3](#), and [S4](#).

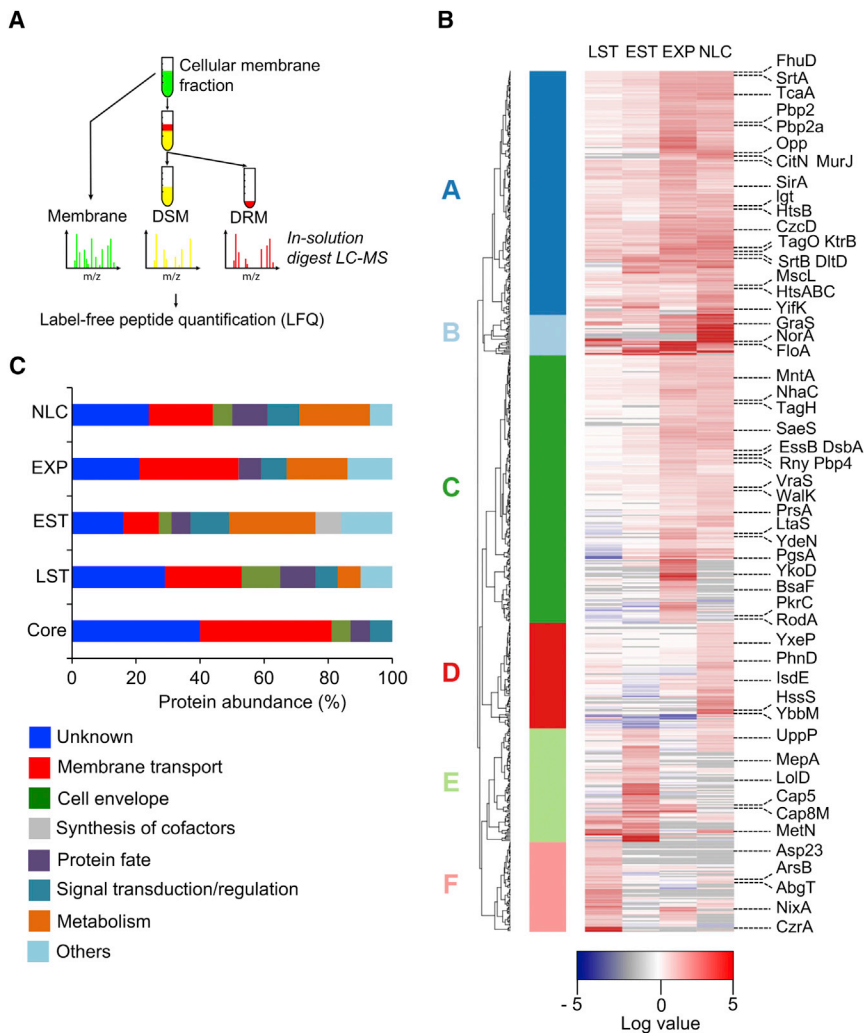


Figure 6. MRSA Proteins Associated with the FMM-Rich Fraction

(A) Workflow of membrane protein extraction and label-free quantification (LFQ) analyses of FMM-enriched associated proteins.

(B) MS-based LFQ of the DRM fraction proteome of four growth conditions (LST, late stationary; EST, early stationary; EXP, exponential; and NLC, nutrient-limiting conditions). Heatmap shows ratios of calculated protein abundance in DRM versus total membrane proteome and DSM versus total membrane proteome by unsupervised hierarchical clustering. Red denotes a DRM increase relative to total membrane proteome and blue, a decrease. Gray boxes indicate missing values. A number of proteins are highlighted. Clusters A (dark blue) and B (light blue) comprise proteins enriched in DRM in all growth conditions. Cluster C (dark green) shows DRM proteins in EXP, cluster D (red) in NLC, cluster E (light green) in EST, cluster F (pink) in LST.

(C) Functional classification of DRM-associated proteins according to TIGRFAMM in four growth conditions and a core of proteins detected in all conditions tested.

See also [Figure S5](#) and [Table S4](#).

PBP2a oligomerization. FMM architectural alterations thus appear to compromise PBP2a oligomerization.

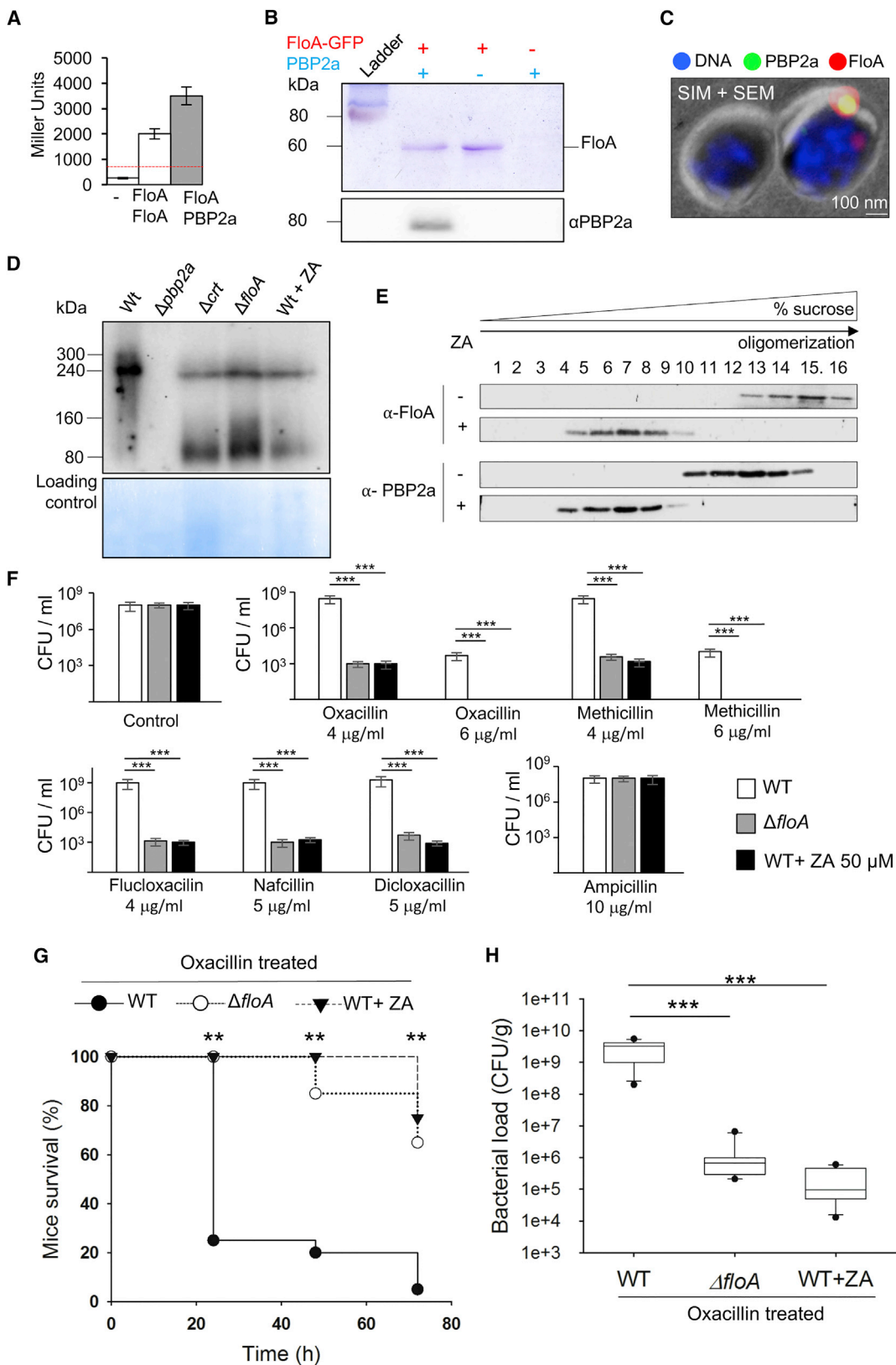
Based on this finding, we designed an approach to exogenously perturb PBP2a oligomerization by inhibiting biosynthesis of FMM-constituent lipids using cholesterol-lowering drugs (statins) ([Figure S6C](#)). Statins inhibit the mevalonate pathway, and thus cholesterol synthesis, in patients with hypercholesterolemia. *S. aureus* uses the mevalonate pathway to produce

scaffold proteins stabilize protein complexes by tethering interacting partners ([Good et al., 2011](#)); a likely effect of flotillin on PBP2a activity would be FloA promotion of more efficient PBP2a oligomerization with interacting partners. Using a bacterial three-hybrid (B3H) assay, we measured PBP2a interaction with the potential partners PrsA, RodA, or PBP2 in strains that produced low, medium, or high FloA levels ([Figure S6B](#)). Interaction of PBP2a and protein partners clearly improved at low and medium FloA concentrations, while a slight decrease was detected at high FloA levels. This finding is consistent with the fact that optimal scaffold concentration tethers interaction partners, whereas high concentrations titrate interacting partners and inhibit interaction, thus indicating that FloA behaves as a scaffold protein ([Good et al., 2011](#)). We analyzed oligomerization of PBP2a (~80 kDa) in *S. aureus* cells using BN-PAGE, followed by PBP2a immunodetection ([Figure 7D](#)). We identified signals (~240 and 300 kDa) in WT that were absent in Δ *pbp2a* samples (or Δ *mecA*), attributable to PBP2a oligomerization. These bands were less intense in Δ *floA* and Δ *crt* mutants, concurrent with additional bands at ~80 and ~160 kDa that correspond to partial

staphyloxanthin; thus, statins inhibit staphyloxanthin biosynthesis ([Liu et al., 2008](#)) ([Figure S6D](#)). When treated with the statin zaragozic acid (ZA, 50 μ M), *S. aureus* cells showed no growth defects ([Figures S7A](#) and [S7B](#)), but the number of FloA membrane foci was reduced ([Figure S7C](#)) ([López and Kolter, 2010](#)). When ZA-treated MRSA cells were tested for PBP2a oligomerization using BN-PAGE ([Figure 7D](#)), we detected bands at ~80 kDa, which denoted deficient PBP2a oligomerization. The membrane fraction of untreated and ZA-treated *S. aureus* cells was resolved by velocity sucrose gradient centrifugation ([Figure 7E](#)). FloA and PBP2a immunodetection in WT samples showed both signals concentrated in high-density sucrose fractions, where high-MW protein complexes were detected. In contrast, ZA-treated samples showed signals in low-density sucrose fractions, in which low-MW protein complexes were detected, denoting reduced oligomerization of flotillin and PBP2a in ZA-treated MRSA.

FMM Disruption Inhibits Penicillin Resistance in MRSA

Evidence that FMM perturbation affects PBP2a oligomerization led us to test whether β -lactam antibiotics inhibit growth of a



(legend on next page)

MRSA $\Delta floA$ mutant. Cultures of WT and the $\Delta floA$ mutant were incubated with various β -lactam antibiotics (methicillin, oxacillin, flucoxacin, nafcillin, and dicloxacillin), which are normally used to treat methicillin-sensitive *S. aureus* (MSSA) infections but do not eradicate MRSA infections (Peacock and Paterson, 2015) (Figure 7F). We detected severe growth inhibition in $\Delta floA$ compared to WT samples at antibiotic concentrations that typically inhibit MSSA growth. As controls, WT and $\Delta floA$ showed comparable resistance to ampicillin, as resistance to this β -lactam antibiotic is via secretion of a β -lactamase rather than via PBP2a (Ayliffe, 1963). We then compared β -lactam sensitivity of untreated and ZA-treated MRSA cultures (Figure 7F). The antibiotic sensitivity profiles of ZA-treated cultures resembled those of the $\Delta floA$ mutant, as did those of other statin molecules (Figures S7D–S7F), which indicates that disturbance of the FMM interferes with penicillin resistance in MRSA.

To determine whether MRSA penicillin sensitivity can be achieved in an *in vivo* infection, we compared the infective potential of WT and $\Delta floA$ strains in a murine infection model. Infected mice ($n = 10$; 3×10^7 colony-forming units [CFU]) were treated with oxacillin (200 mg/kg/day) (Hertlein et al., 2014) and the survival rate was monitored 3 days post infection (Figure 7G). Mice infected with the WT strain showed higher mortality (10% survival rate) than those infected with a $\Delta floA$ mutant (70% survival rate; $p < 0.01$). To compare antibiotic sensitivity of untreated and ZA-treated WT cells, infected mice ($n = 10$; 3×10^7 CFU) were treated with oxacillin (200 mg/kg/day) or with a combination of oxacillin (200 mg/kg/day) and ZA (50 mg/kg/day); survival was monitored as before (Figures 7G and S7G). Infected mice treated with oxacillin and ZA had a significantly higher survival rate ($p < 0.01$) than those treated with oxacillin alone. In another experiment, a MRSA strain isolated from a pneumonia patient (López-Collazo et al., 2015) was used to infect mice intranasally ($n = 10$; 3×10^8 CFU) prior to oxacillin treatment (200 mg/kg/day) or treatment with oxacillin (200 mg/kg/day) and ZA (50 mg/kg/day) (Figure 7H). Infections were allowed to progress for 2 days before lungs were collected and bacterial load counted. Infected mice treated with a combination of oxacillin and ZA showed significantly reduced bacterial load ($p < 0.001$) compared to oxacillin-treated mice.

DISCUSSION

Evidence for the importance of membrane lipid domains in bacterial cell organization is increasing (García-Lara et al., 2015; Nickels et al., 2017). Here, we used the human pathogen MRSA to characterize bacterial FMMs structurally and functionally. FMM-constituent lipids are isoprenoid saccharolipids derived from the carotenoid staphyloxanthin. The scaffold protein flotillin preferentially binds these lipids and oligomerizes in staphyloxanthin-rich membrane microdomains. In a similar manner, eukaryotic lipid rafts are also constituted by glucolipids (sphingolipids) (Simons and Toomre, 2000). Differences in glucolipid headgroup structure dictates their lateral segregation in microdomains within the phospholipid membrane, whereas hydrogen bonding between headgroup sugars stabilizes glucolipid interactions for microdomain rigidity (Rock et al., 1990; Thompson and Tillack, 1985). Such headgroup structure differences of constituent lipids enabled us to visualize FMMs using electron microscopy techniques and uranyl acetate staining; we recognized these regions as light electron-dense membrane areas to which flotillin localizes preferentially and attracts a number of multimeric protein complexes.

We used FloA-mediated PBP2a oligomerization to demonstrate the biological significance of FMMs. FloA scaffold activity promotes efficient PBP2a oligomerization, and lack of flotillin inhibits PBP2a hetero-oligomerization, probably preceding FtsZ recruitment. This scaffold activity might contribute to oligomerization of other FMM-associated proteins, which could explain the virulence defect in flotillin mutants of *C. jejuni* (Tareen et al., 2013) or *B. anthracis* (Somani et al., 2016), as well as the thylakoid organization defect in cyanobacteria (Bryan et al., 2011).

When studying the influence of FMM organization on PBP2a, we observed that perturbation of FMM architecture affects PBP2a oligomerization and reduces MRSA proliferative capacity in the presence of β -lactam antibiotics. Repurposing statins, currently used to treat hypercholesterolemia, to inhibit the biosynthesis of FMM-constituent lipids led to interference in FMM assembly in MRSA. As a result, statin-treated MRSA infections became susceptible to conventional antibiotic therapy in a mouse model.

Our results help to explain clinical studies that detected a beneficial role of statins in microbial infections (Falagas et al.,

Figure 7. Flotillin Scaffolds PBP2a Oligomerization

- (A) B2H analysis showing FloA-PBP2a interaction. Minus sign indicates empty plasmids (negative control). FloA-FloA interaction is positive control. Red line denotes 700-Miller-unit threshold to define interaction (BACTH System; EuroMedex). Data shown as mean \pm SD for three independent biological replicates ($n = 3$).
- (B) PBP2a immunodetection in protein samples pulled down with FloA-GFP (+/+ lane). Negative controls are FloA-GFP-labeled $\Delta pbp2a$ (or $\Delta mecA$) strain (+/- lane) and unlabeled WT strain (-/- lane).
- (C) srAT (SIM + Scan-EM) to detect FloA-PBP2a colocalization in 100-nm sections. When detected in thin sections, PBP2a colocalized with flotillin.
- (D) BN-PAGE and immunoblot of PBP2a oligomeric states of various mutants. WT + ZA shows membrane fraction of ZA-treated WT cells. Arrowheads indicate oligomeric species at 240 and 80 kDa.
- (E) Immunoblot of FloA and PBP2a oligomerization in membrane fractions from untreated or ZA-treated WT cells resolved on sucrose gradients.
- (F) Effect of MRSA resistance to several β -lactam antibiotics using WT, $\Delta floA$, and ZA-treated WT samples. Data shown as mean \pm SD for three independent experiments ($n = 3$). Statistical analysis, one-way ANOVA with Tukey's test for multiple comparisons, *** $p < 0.001$.
- (G) Survival curve of oxacillin-treated mice infected with WT, $\Delta floA$ mutant, or ZA-treated WT (3×10^7 cells, $n = 10$). Statistical analysis, one-way ANOVA with Tukey's comparison between WT versus $\Delta floA$ or WT versus WT+ZA, ** $p < 0.01$. Each point represents the mean of three independent experiments.
- (H) Bacterial load in lungs of oxacillin-treated infected mice in a pulmonary infection model. Mice were infected with 3×10^8 cells ($n = 10$). 2 days after bacterial challenge, organs were collected aseptically and CFUs counted. Statistical analysis, one-way ANOVA with Tukey's comparison, *** $p < 0.001$.

2008; Liappis et al., 2001; López-Cortés et al., 2013; Parihar et al., 2014). In addition, our work could contribute a context for the interpretation of *in vitro* studies that did not detect an antimicrobial effect of statins in specific conditions or bacterial species (Bergman et al., 2011; Wan et al., 2014). Statin-mediated FMM dispersal requires production of FMM-constituent lipids via the mevalonate pathway, which is not universal in bacteria (Heuston et al., 2012). Moreover, our study shows that statins cause FMM dispersal and thus do not have intrinsic bactericidal activity; rather, they interfere with bacterial processes and synergize with other antimicrobials to kill pathogens.

The organization of FMM platforms, which in some structural and functional aspects resemble lipid rafts of eukaryotic cells, reveals a remarkable level of sophistication that is unexpected in bacteria. Disassembly of these platforms in pathogens such as MRSA could simultaneously affect numerous infection-related processes, including inhibition of antibiotic resistance, and could thus be used in the development of antimicrobial therapies for multidrug-resistant bacteria.

STAR★METHODS

Detailed methods are provided in the online version of this paper and include the following:

- KEY RESOURCES TABLE
- CONTACT FOR REAGENTS AND RESOURCE SHARING
- EXPERIMENTAL MODEL AND SUBJECT DETAILS
 - Strains, media, and culture conditions
- METHOD DETAILS
 - Construction of knock-out mutants
 - Generation of labeled strains
 - Flotillin expression and purification
 - Cell fractionation and purification of DRM
 - Lipid analysis by UPLC-ESI-qTOF-MS
 - Purification of staphyloxanthin lipids
 - Thin-layer chromatography
 - Lectin binding assay
 - Small unilamellar vesicle preparation
 - Bio-layer interferometry
 - Liposome-flotation binding assay
 - Sucrose gradients
 - Size exclusion chromatography
 - Fluorescence microscopy
 - Direct stochastic optical reconstruction microscopy
 - Correlative light and electron microscopy
 - Electron tomography
 - Immunogold FloA detection
 - Lipid-protein complex analysis by electron microscopy
 - Label-free protein quantification by mass spectrometry
 - Bacterial two-hybrid analysis
 - Bacterial three-hybrid analysis
 - Pull-down assay
 - Blue-native PAGE
 - Western blot analysis and immunodetection
 - Mouse infection studies
 - Software used in this study

● QUANTIFICATION AND STATISTICAL ANALYSIS

- Statistical analyses

● DATA AND SOFTWARE AVAILABILITY

- Data availability

SUPPLEMENTAL INFORMATION

Supplemental Information includes seven figures, four tables, and three movies and can be found with this article online at <https://doi.org/10.1016/j.cell.2017.10.012>.

AUTHOR CONTRIBUTIONS

Conceptualization, D.L.; Methodology, A.F., S.G., C.S., and D.L.; Investigation, E.G.-F., G.K., R.M.W., A.F., S.T.S., J.S., B.M.-S., S.G., S.M.M., C.S., and D.L.; Writing—Original Draft, D.L.; Review and Editing, E.G.-F., G.K., R.M.W., A.F., S.T.S., J.S., B.M.-S., S.G., S.M.M., C.S., and D.L.; Funding Acquisition, Resources, and Supervision, D.L.

ACKNOWLEDGMENTS

G.K. received a fellowship from the FWF (Austria); E.G.-F. from the JdC (Spain); B.M.-S. from the University of Würzburg (Germany), and S.M.M. from the Studienstiftung d. dt. Volkes (Germany). We thank C. Mark for editorial assistance. This work was funded by ERC335568 (EU) and BFU2014-55601-P (Spain) to D.L.

Received: May 31, 2017

Revised: September 18, 2017

Accepted: October 6, 2017

Published: November 2, 2017

REFERENCES

- Arnaud, M., Chastanet, A., and Débarbouillé, M. (2004). New vector for efficient allelic replacement in naturally nontransformable, low-GC-content, gram-positive bacteria. *Appl. Environ. Microbiol.* **70**, 6887–6891.
- Ayliffe, G.A. (1963). Ampicillin inactivation and sensitivity of coliform bacilli. *J. Gen. Microbiol.* **30**, 339–348.
- Bach, J.N., and Bramkamp, M. (2013). Flotillins functionally organize the bacterial membrane. *Mol. Microbiol.* **88**, 1205–1217.
- Bach, J.N., and Bramkamp, M. (2015). Dissecting the molecular properties of prokaryotic flotillins. *PLoS ONE* **10**, e0116750.
- Bergman, P., Linde, C., Pütsep, K., Pohanka, A., Normark, S., Henriques-Normark, B., Andersson, J., and Björkhem-Bergman, L. (2011). Studies on the antibacterial effects of statins—in vitro and in vivo. *PLoS ONE* **6**, e24394.
- Bickel, P.E., Scherer, P.E., Schnitzer, J.E., Oh, P., Lisanti, M.P., and Lodish, H.F. (1997). Flotillin and epidermal surface antigen define a new family of caveolae-associated integral membrane proteins. *J. Biol. Chem.* **272**, 13793–13802.
- Bramkamp, M., and Lopez, D. (2015). Exploring the existence of lipid rafts in bacteria. *Microbiol. Mol. Biol. Rev.* **79**, 81–100.
- Brown, D.A. (2002). Isolation and use of rafts. In *Curr Protoc Immunol* (John Wiley & Sons).
- Bryan, S.J., Burroughs, N.J., Evered, C., Sacharz, J., Nennering, A., Mullineaux, C.W., and Spence, E.M. (2011). Loss of the SPHF homologue Sir1768 leads to a catastrophic failure in the maintenance of thylakoid membranes in *Synechocystis* sp. PCC 6803. *PLoS ONE* **6**, e19625.
- Cho, H., Wivagg, C.N., Kapoor, M., Barry, Z., Rohs, P.D., Suh, H., Marto, J.A., Garner, E.C., and Bernhardt, T.G. (2016). Bacterial cell wall biogenesis is mediated by SEDS and PBP polymerase families functioning semi-autonomously. *Nat. Microbiol.* **1**.
- Donovan, C., and Bramkamp, M. (2009). Characterization and subcellular localization of a bacterial flotillin homologue. *Microbiology* **155**, 1786–1799.

- Falagas, M.E., Makris, G.C., Matthaiou, D.K., and Rafailidis, P.I. (2008). Statins for infection and sepsis: a systematic review of the clinical evidence. *J. Antimicrob. Chemother.* *61*, 774–785.
- Feng, X., Hu, Y., Zheng, Y., Zhu, W., Li, K., Huang, C.H., Ko, T.P., Ren, F., Chan, H.C., Nega, M., et al. (2014). Structural and functional analysis of *Bacillus subtilis* YisP reveals a role of its product in biofilm production. *Chem. Biol.* *21*, 1557–1563.
- Fishovitz, J., Hermoso, J.A., Chang, M., and Mobashery, S. (2014). Penicillin-binding protein 2a of methicillin-resistant *Staphylococcus aureus*. *IUBMB Life* *66*, 572–577.
- García-Lara, J., Weihs, F., Ma, X., Walker, L., Chaudhuri, R.R., Kasturiarachchi, J., Crossley, H., Golestanian, R., and Foster, S.J. (2015). Supramolecular structure in the membrane of *Staphylococcus aureus*. *Proc. Natl. Acad. Sci. USA* *112*, 15725–15730.
- Gautam, S., Kim, T., and Spiegel, D.A. (2015). Chemical probes reveal an extraseptal mode of cross-linking in *Staphylococcus aureus*. *J. Am. Chem. Soc.* *137*, 7441–7447.
- Ghodke, R.M., Tour, N., and Devi, K. (2012). Effects of statins and cholesterol on memory functions in mice. *Metab. Brain Dis.* *27*, 443–451.
- Good, M.C., Zalatan, J.G., and Lim, W.A. (2011). Scaffold proteins: hubs for controlling the flow of cellular information. *Science* *332*, 680–686.
- Hayat, M.A. (1993). *Stains and cytochemical methods* (New York, London: Plenum Press).
- Heimesaat, M.M., Lugert, R., Fischer, A., Alutis, M., Kühl, A.A., Zautner, A.E., Tareen, A.M., Göbel, U.B., and Bereswill, S. (2014). Impact of *Campylobacter jejuni* cj0268c knockout mutation on intestinal colonization, translocation, and induction of immunopathology in gnotobiotic IL-10 deficient mice. *PLoS ONE* *9*, e90148.
- Helmprobst, F., Frank, M., and Stigloher, C. (2015). Presynaptic architecture of the larval zebrafish neuromuscular junction. *J. Comp. Neurol.* *523*, 1984–1997.
- Hertlein, T., Sturm, V., Lorenz, U., Sumathy, K., Jakob, P., and Ohlsen, K. (2014). Bioluminescence and 19F magnetic resonance imaging visualize the efficacy of lysostaphin alone and in combination with oxacillin against *Staphylococcus aureus* in murine thigh and catheter-associated infection models. *Antimicrob. Agents Chemother.* *58*, 1630–1638.
- Heuston, S., Begley, M., Gahan, C.G., and Hill, C. (2012). Isoprenoid biosynthesis in bacterial pathogens. *Microbiology* *158*, 1389–1401.
- Jousselin, A., Renzoni, A., Andrey, D.O., Monod, A., Lew, D.P., and Kelley, W.L. (2012). The posttranslational chaperone lipoprotein PrsA is involved in both glycopeptide and oxacillin resistance in *Staphylococcus aureus*. *Antimicrob. Agents Chemother.* *56*, 3629–3640.
- Jousselin, A., Manzano, C., Biette, A., Reed, P., Pinho, M.G., Rosato, A.E., Kelley, W.L., and Renzoni, A. (2015). The *Staphylococcus aureus* Chaperone PrsA Is a New Auxiliary Factor of Oxacillin Resistance Affecting Penicillin-Binding Protein 2A. *Antimicrob. Agents Chemother.* *60*, 1656–1666.
- Koch, G., Wermser, C., Acosta, I.C., Kricks, L., Stengel, S.T., Yepes, A., and Lopez, D. (2017). Attenuating *Staphylococcus aureus* Virulence by Targeting Flotillin Protein Scaffold Activity. *Cell Chem Biol* *24*, 845–857 e6.
- Kraft, M.L. (2013). Plasma membrane organization and function: moving past lipid rafts. *Mol. Biol. Cell* *24*, 2765–2768.
- Kreiswirth, B., Kornblum, J., Arbeit, R.D., Eisner, W., Maslow, J.N., McGeer, A., Low, D.E., and Novick, R.P. (1993). Evidence for a clonal origin of methicillin resistance in *Staphylococcus aureus*. *Science* *259*, 227–230.
- Kullik, I., Giachino, P., and Fuchs, T. (1998). Deletion of the alternative sigma factor sigmaB in *Staphylococcus aureus* reveals its function as a global regulator of virulence genes. *J. Bacteriol.* *180*, 4814–4820.
- LaRocca, T.J., Pathak, P., Chiantia, S., Toledo, A., Silvius, J.R., Benach, J.L., and London, E. (2013). Proving lipid rafts exist: membrane domains in the prokaryote *Borrelia burgdorferi* have the same properties as eukaryotic lipid rafts. *PLoS Pathog.* *9*, e1003353.
- Łeski, T.A., and Tomasz, A. (2005). Role of penicillin-binding protein 2 (PBP2) in the antibiotic susceptibility and cell wall cross-linking of *Staphylococcus aureus*: evidence for the cooperative functioning of PBP2, PBP4, and PBP2A. *J. Bacteriol.* *187*, 1815–1824.
- Liappis, A.P., Kan, V.L., Rochester, C.G., and Simon, G.L. (2001). The effect of statins on mortality in patients with bacteremia. *Clin. Infect. Dis.* *33*, 1352–1357.
- Liu, C.I., Liu, G.Y., Song, Y., Yin, F., Hensler, M.E., Jeng, W.Y., Nizet, V., Wang, A.H., and Oldfield, E. (2008). A cholesterol biosynthesis inhibitor blocks *Staphylococcus aureus* virulence. *Science* *319*, 1391–1394.
- López, D., and Kolter, R. (2010). Functional microdomains in bacterial membranes. *Genes Dev.* *24*, 1893–1902.
- López-Collazo, E., Jurado, T., de Dios Caballero, J., Pérez-Vázquez, M., Vindel, A., Hernández-Jiménez, E., Tamames, J., Cubillos-Zapata, C., Manrique, M., Tobes, R., et al. (2015). In vivo attenuation and genetic evolution of a ST247-SCCmecI MRSA clone after 13 years of pathogenic bronchopulmonary colonization in a patient with cystic fibrosis: implications of the innate immune response. *Mucosal Immunol.* *8*, 362–371.
- López-Cortés, L.E., Gálvez-Acebal, J., Del Toro, M.D., Velasco, C., de Cueto, M., Caballero, F.J., Muniain, M.A., Pascual, A., and Rodríguez-Baño, J. (2013). Effect of statin therapy in the outcome of bloodstream infections due to *Staphylococcus aureus*: a prospective cohort study. *PLoS ONE* *8*, e82958.
- Lorent, J.H., and Levental, I. (2015). Structural determinants of protein partitioning into ordered membrane domains and lipid rafts. *Chem. Phys. Lipids* *192*, 23–32.
- Markert, S.M., Britz, S., Proppert, S., Lang, M., Witvliet, D., Mulcahy, B., Sauer, M., Zhen, M., Bessereau, J.L., and Stigloher, C. (2016). Filling the gap: adding super-resolution to array tomography for correlated ultrastructural and molecular identification of electrical synapses at the *C. elegans* connectome. *Neurophotonics* *3*, 041802.
- Marshall, J.H., and Wilmoth, G.J. (1981). Proposed pathway of triterpenoid carotenoid biosynthesis in *Staphylococcus aureus*: evidence from a study of mutants. *J. Bacteriol.* *147*, 914–919.
- Martos, A., Raso, A., Jiménez, M., Petrášek, Z., Rivas, G., and Schwille, P. (2015). FtsZ Polymers Tethered to the Membrane by ZipA Are Susceptible to Spatial Regulation by Min Waves. *Biophys. J.* *108*, 2371–2383.
- McDougal, L.K., Steward, C.D., Killgore, G.E., Chaitram, J.M., McAllister, S.K., and Tenover, F.C. (2003). Pulsed-field gel electrophoresis typing of oxacillin-resistant *Staphylococcus aureus* isolates from the United States: establishing a national database. *J. Clin. Microbiol.* *41*, 5113–5120.
- McQuillen, K. (1962). Bacterial Ribosomes and Protein Synthesis. *J. Gen. Microbiol.* *29*, 53–57.
- Monteiro, J.M., Fernandes, P.B., Vaz, F., Pereira, A.R., Tavares, A.C., Ferreira, M.T., Pereira, P.M., Veiga, H., Kuru, E., VanNieuwenhze, M.S., et al. (2015). Cell shape dynamics during the staphylococcal cell cycle. *Nat. Commun.* *6*, 8055.
- Nickels, J.D., Chatterjee, S., Stanley, C.B., Qian, S., Cheng, X., Myles, D.A.A., Standaert, R.F., Elkins, J.G., and Katsaras, J. (2017). The in vivo structure of biological membranes and evidence for lipid domains. *PLoS Biol.* *15*, e2002214.
- Otero, L.H., Rojas-Altuve, A., Llarrull, L.I., Carrasco-López, C., Kumarasiri, M., Lastochkin, E., Fishovitz, J., Dawley, M., Heseck, D., Lee, M., et al. (2013). How allosteric control of *Staphylococcus aureus* penicillin binding protein 2a enables methicillin resistance and physiological function. *Proc. Natl. Acad. Sci. USA* *110*, 16808–16813.
- Palade, G.E. (1955). A small particulate component of the cytoplasm. *J. Biophys. Biochem. Cytol.* *1*, 59–68.
- Parihar, S.P., Guler, R., Khutlang, R., Lang, D.M., Hurdal, R., Mhlanga, M.M., Suzuki, H., Marais, A.D., and Brombacher, F. (2014). Statin therapy reduces the *Mycobacterium tuberculosis* burden in human macrophages and in mice by enhancing autophagy and phagosome maturation. *J. Infect. Dis.* *209*, 754–763.
- Peacock, S.J., and Paterson, G.K. (2015). Mechanisms of Methicillin Resistance in *Staphylococcus aureus*. *Annu. Rev. Biochem.* *84*, 577–601.

- Pelz, A., Wieland, K.P., Putzbach, K., Hentschel, P., Albert, K., and Götz, F. (2005). Structure and biosynthesis of staphyloxanthin from *Staphylococcus aureus*. *J. Biol. Chem.* *280*, 32493–32498.
- Pinho, M.G., de Lencastre, H., and Tomasz, A. (2001a). An acquired and a native penicillin-binding protein cooperate in building the cell wall of drug-resistant staphylococci. *Proc. Natl. Acad. Sci. USA* *98*, 10886–10891.
- Pinho, M.G., Filipe, S.R., de Lencastre, H., and Tomasz, A. (2001b). Complementation of the essential peptidoglycan transpeptidase function of penicillin-binding protein 2 (PBP2) by the drug resistance protein PBP2A in *Staphylococcus aureus*. *J. Bacteriol.* *183*, 6525–6531.
- Rock, P., Allietta, M., Young, W.W., Jr., Thompson, T.E., and Tillack, T.W. (1990). Organization of glycosphingolipids in phosphatidylcholine bilayers: use of antibody molecules and Fab fragments as morphologic markers. *Biochemistry* *29*, 8484–8490.
- Schneider, J., Yepes, A., Garcia-Betancur, J.C., Westedt, I., Mielich, B., and López, D. (2012). Streptomycin-induced expression in *Bacillus subtilis* of YtnP, a lactonase-homologous protein that inhibits development and streptomycin production in *Streptomyces griseus*. *Appl. Environ. Microbiol.* *78*, 599–603.
- Schneider, J., Klein, T., Mielich-Süss, B., Koch, G., Franke, C., Kuipers, O.P., Kovács, A.T., Sauer, M., and Lopez, D. (2015). Spatio-temporal remodeling of functional membrane microdomains organizes the signaling networks of a bacterium. *PLoS Genet.* *11*, e1005140.
- Silva-Rocha, R., Martínez-García, E., Calles, B., Chavarría, M., Arce-Rodríguez, A., de Las Heras, A., Páez-Espino, A.D., Durante-Rodríguez, G., Kim, J., Nikel, P.I., et al. (2013). The Standard European Vector Architecture (SEVA): a coherent platform for the analysis and deployment of complex prokaryotic phenotypes. *Nucleic Acids Res.* *41*, D666–D675.
- Simons, K., and Ikonen, E. (1997). Functional rafts in cell membranes. *Nature* *387*, 569–572.
- Simons, K., and Toomre, D. (2000). Lipid rafts and signal transduction. *Nat. Rev. Mol. Cell Biol.* *1*, 31–39.
- Singer, S.J., and Nicolson, G.L. (1972). The fluid mosaic model of the structure of cell membranes. *Science* *175*, 720–731.
- Somani, V.K., Aggarwal, S., Singh, D., Prasad, T., and Bhatnagar, R. (2016). Identification of Novel Raft Marker Protein, FlotP in *Bacillus anthracis*. *Front. Microbiol.* *7*, 169.
- Tareen, A.M., Lüder, C.G., Zautner, A.E., Groß, U., Heimesaat, M.M., Bereswill, S., and Lugert, R. (2013). The *Campylobacter jejuni* Cj0268c protein is required for adhesion and invasion in vitro. *PLoS ONE* *8*, e81069.
- Thompson, T.E., and Tillack, T.W. (1985). Organization of glycosphingolipids in bilayers and plasma membranes of mammalian cells. *Annu. Rev. Biophys. Biophys. Chem.* *14*, 361–386.
- Ting-Beall, H.P. (1980). Interactions of uranyl ions with lipid bilayer membranes. *J. Microsc.* *118*, 221–227.
- Wan, Y.D., Sun, T.W., Kan, Q.C., Guan, F.X., and Zhang, S.G. (2014). Effect of statin therapy on mortality from infection and sepsis: a meta-analysis of randomized and observational studies. *Crit. Care* *18*, R71.
- Wieland, B., Feil, C., Gloria-Maercker, E., Thumm, G., Lechner, M., Bravo, J.M., Poralla, K., and Götz, F. (1994). Genetic and biochemical analyses of the biosynthesis of the yellow carotenoid 4,4'-diaponeurosporene of *Staphylococcus aureus*. *J. Bacteriol.* *176*, 7719–7726.
- Wittig, I., Braun, H.P., and Schagger, H. (2006). Blue native PAGE. *Nat. Protoc.* *1*, 418–428.
- Yepes, A., Koch, G., Waldvogel, A., Garcia-Betancur, J.C., and Lopez, D. (2014). Reconstruction of mreB expression in *Staphylococcus aureus* via a collection of new integrative plasmids. *Appl. Environ. Microbiol.* *80*, 3868–3878.
- Zapun, A., Contreras-Martel, C., and Vernet, T. (2008). Penicillin-binding proteins and beta-lactam resistance. *FEMS Microbiol. Rev.* *32*, 361–385.

STAR★METHODS

KEY RESOURCES TABLE

REAGENT or RESOURCE	SOURCE	IDENTIFIER
Antibodies		
α -FloA chicken	Davids	This study
α -FLAG rabbit	Sigma	Cat# F7425; RRID: AB_439687
α -GroEL rabbit	Sigma	Cat# G6532; RRID: AB_259939
α -chicken HRP-conjugated secondary	Thermo Scientific	Cat# A1654
α -rabbit HRP-conjugated secondary	BioRad	Cat# 1706515; RRID: AB_2617112
α -PBP2a rabbit	RayBiotech	Cat# 130-10073-100
α -rabbit-Cy5 conjugated secondary	Abcam	Cat# Ab97077; RRID: AB_10679461
α -chicken-Cy3 conjugated secondary	Abcam	Cat# Ab97145; RRID: AB_10679516
α -chicken-Gold 10 nm diameter conjugated secondary	BBI solutions	Cat# EM.RCHL.10
α -chicken Alexa Fluor 488 conjugated secondary	Thermo Scientific	Cat# A-11029; RRID: AB_2534088
Bacterial and Virus Strains		
List of <i>E. coli</i> strains related to protein production, B2H and B3H assays is in Table S4	This study	N/A
<i>S. aureus</i> ST24R	(López-Collazo et al., 2015)	N/A
<i>S. aureus</i> USA300LAC (WT)	(McDougal et al., 2003)	N/A
<i>S. aureus</i> Δ <i>floA</i>	This study	N/A
<i>S. aureus</i> Δ <i>crt</i>	This study	N/A
<i>S. aureus</i> Δ <i>mecA</i> (Δ <i>pbp2a</i>)	This study	N/A
<i>S. aureus</i> WT FloA-YFP	This study	N/A
<i>S. aureus</i> Δ <i>crt</i> FloA-YFP	This study	N/A
<i>S. aureus</i> WT MAR-YFP	This study	N/A
<i>S. aureus</i> WT PHB-YFP	This study	N/A
<i>S. aureus</i> WT EA4-YFP	This study	N/A
<i>S. aureus</i> WT FloA-SNAP	This study	N/A
<i>S. aureus</i> WT FloA-His6	This study	N/A
<i>S. aureus</i> WT FloA-FLAG	This study	N/A
Chemicals, Peptides, and Recombinant Proteins		
TLC silica gel 60	Merck	Cat#1.05559.0001
Lectin Kit Fluorescein	Vector Laboratories	Cat#FLK-2100
Fluorescein <i>Solanum tuberosum</i> (potato) Lectin	Vector Laboratories	Cat#FL-1161
Superose 6 increase 10/300 GL column	General Electric	Cat# 29-0915-96
Phosphatidylethanolamine	Sigma	Cat#P8068
Phosphatidylglycerol	Sigma	Cat#P8318
Uranyl acetate	Electron Microscopy Sciences	Cat#22400
TMR-Star	New England Biolabs	Cat#S9105S
Ni-NTA resin	QIAGEN	Cat#30210
n-Dodecyl β -D-maltoside	Glycon Biochem	Cat#D97002-C
cOMplete Protease Inhibitor Cocktail	Roche	Cat#11697498001
Zaragozic acid	Santa Cruz	Cat#144541-82-2
Lovastatin	Axxora	Cat#LKT-M1687-M
Mevastatin	Axxora	Cat#LKT-M1685-M
Pravastatin	Axxora	Cat#LKT-P6801-M

(Continued on next page)

Continued

REAGENT or RESOURCE	SOURCE	IDENTIFIER
Simvastatin	Axxora	Cat#LKT-S3449-M
Atorvastatin	Axxora	Cat#LKT-A7658-M
Fluvastatin	Axxora	Cat#LKT-F4482-M
Oxacillin	Sigma	Cat#28221
Methicillin	Sigma	Cat#51454
Flucoxacillin	Sigma	Cat#SML1023
Nafcillin	Sigma	Cat#N3269
Dicloxacillin	Sigma	Cat#D9016
Critical Commercial Assays		
MEM Cell Lytic assay	Sigma	Cat#CE0050
BACTH System Kit	EuroMedex	Cat#EUK001
Chemiluminescent substrate Kit	Thermo-Scientific	Cat#34080
Native polyacrylamide gel system	Invitrogen	Cat# BN1001BOX
Experimental Models: Organisms/Strains		
Mice: BALB/C	Charles River Laboratory	Strain code 028
Oligonucleotides		
See Table S4 for list of primers used in this study	This study	N/A
Recombinant DNA		
pET20b	Novagen	Cat#69739-3
pSNAPf	New England Biolabs	Cat#N9183S
pMAD	(Arnaud et al., 2004)	N/A
pLac	(Yepes et al., 2014)	N/A
pAmy	(Yepes et al., 2014)	N/A
pSEVA621	(Silva-Rocha et al., 2013)	N/A
pSEVA631	(Silva-Rocha et al., 2013)	N/A
pSEVA641	(Silva-Rocha et al., 2013)	N/A
Software and Algorithms		
LAS (Leica Application suite)	Leica	http://www.leica-microsystems.com/products/microscope-software/
FIJI	SciJava	https://fiji.sc
IMOD	University of Colorado	http://bio3d.colorado.edu/imod/
MaxQuant	Max Planck Institute for Biochemistry	http://www.coxdocs.org/doku.php?id=maxquant:start
MassLynx	Waters	http://www.waters.com/waters/en_US/MassLynx-Mass-Spectrometry-Software-/nav.htm?cid=513164&locale=en_US
ProGenesis QI	Waters	http://www.nonlinear.com/progenesis/qi/
Other		
Proteomic data, analyses, and resources related to proteomic analysis to total membrane DRM and DSM proteome	This paper	ProteomeXchange https://www.ebi.ac.uk/pride Identifier: PRIDE: PXD006546
Original unprocessed images (gels, western blots, microscopy images and movies)	This paper	Mendeley data https://data.mendeley.com/ Reserved DOI: https://doi.org/10.17632/zr92hyx6y5.1
Ultra-performance liquid chromatograph coupled to a quadrupole/time-of-flight hybrid mass spectrometer equipped with electrospray ionization source (UPLC-ESI-qTOF-MS)	Synap	G2 HDMS

(Continued on next page)

Continued

REAGENT or RESOURCE	SOURCE	IDENTIFIER
BLItz system	ForteBio	N/A
Size exclusion chromatography	General Electric Healthcare	Akta Pure
Fluorescence microscope	Leica	DMI6000B
dSTORM	ZEISS	Elyra S.1.
Electron Microscope (CLEM)	JEOL	JSM-7500F
Electron Microscope (tomography)	JEOL	JEM-2100
Electron Microscope (Immunogold)	JEOL	JEM 1011
NanoLC-MS/MS	Thermo Scientific	Orbitrap Fusion instrument equipped with an EASY-Spray ion source and coupled to an EASY-nLC 1000

CONTACT FOR REAGENTS AND RESOURCE SHARING

Further information and request for resources and reagents should be directed to and will be fulfilled by the Lead Contact, Daniel Lopez (dlopez@cnb.csic.es).

EXPERIMENTAL MODEL AND SUBJECT DETAILS**Strains, media, and culture conditions****Bacterial strains**

All bacterial strains used in this study are listed in [Key Resources Table](#) and [Table S4](#). The methicillin-resistant *Staphylococcus aureus* (MRSA) strain USA300 ([McDougal et al., 2003](#)) was used for all experiments unless otherwise stated. For cloning purposes, *Escherichia coli* strain DH5 α was used and *S. aureus* strain RN4220 served as the recipient for *S. aureus*.

Bacterial growth conditions

S. aureus strains were cultured in TSB medium supplemented with erythromycin (2 μ g/ml) or kanamycin (10 μ g/ml) when appropriate; *E. coli* strains were cultured in LB medium with ampicillin (100 μ g/ml) when required. To avoid precipitation in aqueous solution, stains were prepared in dimethylsulfoxide (DMSO) stock solution and diluted 1:1 in methanol before addition to *S. aureus* cultures.

In vivo experiment conditions

For *in vivo* experiments using animal models, all animal studies were approved by the local government of Lower Franconia, Germany (license n $^{\circ}$ 55.2-DMS-2532-2-57) and performed in strict accordance with the guidelines for animal care and animal experimentation of the German animal protection law and directive 2010/63/EU of the European parliament on the protection of animals used for scientific purposes. Female BALB/c mice (8-10 weeks old, 16-19 g weight) were purchased (Charles River Laboratories), Mice were housed in polypropylene cages in standardized lighting conditions and had *ad libitum* access to food and water.

METHOD DETAILS**Construction of knock-out mutants**

Δcrt and $\Delta floA$ mutants were generated using a two-step recombination process as reported in ([Arnaud et al., 2004](#)). Briefly, $\Delta crt::km$ and $\Delta floA::spc$ deletion cassettes were generated by using long-flanking-homology PCR and cloned into pMAD plasmid ([Arnaud et al., 2004](#)). The resultant plasmids were inserted into *S. aureus* RN4220 by electroporation and propagated in TSB medium (30°C, 200 RPM) with 1 mM IPTG. After 4 h of incubation, the cultures were shifted for two more hours to 42°C and then plated onto TSB complemented with the antibiotic cassette (kanamycin or spectinomycin) and X-Gal. After 48 h of incubation at 42°C, the blue colonies still carrying the plasmid were discarded. White colonies resistant to kanamycin or spectinomycin were checked by PCR to confirm that the deletion cassette was integrated. $\phi 11$ phage lysates were generated from *S. aureus* RN4220 to infect USA300LAC. Clones resistant to kanamycin or spectinomycin were further verified using PCR. Resulting constructs were verified by DNA sequencing. Primers are listed in [Table S4](#).

Generation of labeled strains

FloA-YFP, FloA-SNAP and FloA-His 6 labeled strains were generated using pAmy and pLac plasmids ([Yepes et al., 2014](#)). All strains used bore the genetic constructs chromosomally integrated in *amyE* or *lacA* neutral loci of *S. aureus*. Sequence-validated plasmids were transformed in RN4220 and transduced into USA300 using phage $\phi 11$. Plasmids were integrated into *amyE* or *lacA* as above ([Arnaud et al., 2004](#)).

Flotillin expression and purification

WT, Δ MAR, Δ PHB and Δ EA4 flotillin variants were overexpressed and purified using pET20b vector (Novagen). Primers are listed in Table S4. This plasmid bears a C-terminal His-Tag sequence and a T7 promoter, allowing induction of gene expression using IPTG. For overexpression, plasmids were transformed in *E. coli* BL21-Gold (Novagen). Protein expression was induced with 0.5 mM IPTG and cultures were grown 5 h at 30°C. Cell pellets were resuspended in 50 mM Tris-HCl pH 8, NaCl 200 mM, 5% glycerol buffer containing 1 mM PMSF and protease inhibitors (Roche) and disrupted using a French press. Cell extracts were incubated (1 h, 4°C) with 0.5% DDM (n-docecyl β -D-maltoside) to solubilize membrane proteins and 1% streptomycin sulfate to precipitate DNA, followed by ultracentrifugation (1 h, 100,000 g) to clear the lysate. Lysates were filtered (0.2 μ m) and passed through a Ni-NTA agarose resin (QIAGEN), which was washed and His-tagged proteins eluted with 250–500 mM imidazole; protein purity was analyzed by SDS-PAGE. Proteins were dialyzed to remove imidazole and kept at –20°C. Purification and dialysis buffers contained 0.02% DDM.

Cell fractionation and purification of DRM

Pellets of *S. aureus* TSB cultures were harvested and resuspended in PBS buffer supplemented with 1 mM phenylmethylsulfonyl-fluoride (PMSF) and 5 μ L DNaseI (2000 U/ml). For enzyme lysis of cells, 15 μ L lysostaphin (1 mg/ml) was added and cells incubated (15 min, 37°C). Cell suspensions were disrupted using a French press. Unbroken cells and debris were removed by centrifugation (10 min, 10,000 g, 4°C) and supernatant ultracentrifuged (1 h, 100,000 g) to separate the membrane fraction. The pellet was dissolved (overnight, 4°C) in 100–200 μ L lysis and separation buffer (Sigma). For FMM isolation, the membrane fraction was processed using the CellLytic MEM protein extraction kit (Sigma) (López and Kolter, 2010). Detergent-resistant (DRM) and -sensitive (DSM) fractions were separated according to the manufacturer's protocol. Samples were analyzed by SDS-PAGE.

Lipid analysis by UPLC-ESI-qTOF-MS

After drying samples in vacuum at 60°C, total lipids were isolated from DRM and DSM samples in 100 μ L isopropanol. Samples were analyzed using ultra-performance liquid chromatograph coupled to a quadrupole/time-of-flight hybrid mass spectrometer equipped with electrospray ionization source (UPLC-ESI-qTOF-MS). Processing of chromatograms, peak detection, and integration were performed using MassLynx software (version 4.1, Waters). ProGenesis QI 2.0 (Waters) was used for data preprocessing for untargeted lipidomics and markers were identified with univariate statistical analysis (ANOVA).

Purification of staphyloxanthin lipids

Staphylococcus aureus culture pellets were resuspended in 10 mL methanol and incubated (30 min, 60°C) with continuous agitation. Samples were centrifuged to remove cell debris and the pigment-containing supernatant concentrated in a speedvac. Carotenoids were extracted with 2 mL ethyl acetate/1.7 M NaCl (1:1 v/v). After centrifugation, the ethyl acetate phase containing carotenoids was recovered and the aqueous phase was re-extracted with 0.5 mL ethyl acetate (Pelz et al., 2005). The extract was dried *in vacuo* and the carotenoid powder stored at –20°C.

To purify staphyloxanthin, total carotenoid lipids were resuspended in chloroform and separated by TLC (see below). The staphyloxanthin band (Marshall and Wilmoth, 1981) was scratched off the TLC plates and extracted with 4 mL ethyl acetate/1.7 M NaCl (1:1 v/v) as above. Staphyloxanthin purity was confirmed by analyzing its mass by ESI-TOF-MS and its absorbance by UV-spectrum measurements.

To compare the carotenoid composition of FMM-enriched and -depleted fractions, carotenoid lipids were purified from DRM and DSM fractions by methanol/chloroform/water extraction (1/1/2). DRM and DSM fractions were resuspended in 1 vol H₂O, mixed with 1 vol chloroform and of methanol and centrifuged to separate organic and aqueous phases. The carotenoid-containing chloroform phase was dried *in vacuo* and stored at –20°C.

Thin-layer chromatography

Purified lipids from DRM and DSM fractions were resuspended in chloroform and loaded on silica gel 60 plates (Merck). Pigments were resolved using hexane-acetone (60:40, v/v) as mobile phase. Bands corresponding to staphyloxanthin lipids are detected by their yellow color.

Lectin binding assay

The DRM fraction isolated from *S. aureus* WT and Δ crt mutant were spotted on silica gel 60 plates (Merck-Millipore). Dried plates were blocked with 10% skim milk (TBS-Tween 0.05%, 1 h) and incubated with fluorescein-labeled lectins (Vector Laboratories) to detect sugar moieties, at a final concentration of 6.5 μ g/ml in TBS-Tween 0.05% (overnight, 4°C, mild agitation). Plates were washed (TBS-Tween 0.05%, 2x 30 min) and fluorescence was detected with a Safe Imager blue-light transilluminator (Invitrogen). Samples were light-protected for all incubation steps. Images were analyzed with FIJI.

Small unilamellar vesicle preparation

Solutions of staphyloxanthin, PE (Sigma) and PG (Sigma) in chloroform (0.4 mg) were dried under nitrogen flow (1 min) and kept under vacuum for 2 h. Multilamellar vesicles (MLV) were obtained by hydration in 100 μ L 50 mM Tris-HCl, 150 mM KCl pH 7.5 buffer (final

lipid concentration 4 mg/ml). Small unilamellar vesicles (SUVs) were obtained by sonication of MLV (10–20 min or until the solution was transparent) (Martos et al., 2015). SUV were kept at -20°C .

Bio-layer interferometry

Lipid-protein interactions were measured by bio-layer interferometry using a single channel BLItz system (ForteBio). Staphyloxanthin, PG and PE SUV were sonicated (2 min) and diluted in hydration buffer as above to a final concentration of 1 mM. Flotillin variants were diluted ≥ 20 -fold to a final concentration of 0.5 μM (0.001% DDM). Lipids were immobilized on aminopropylsilane biosensor tips, and flotillin variants were added to the biosensor to estimate the affinity constant (K_D) (room temperature, with vigorous shaking (2200 rpm)). Each binding reaction was constituted by a 30 s baseline (buffer), followed by a 300 s association phase (lipid or protein binding), and a 300 s dissociation phase (buffer only). BLItz Pro software was used to determine rate constants (K_a , K_d) for net association and dissociation, the equilibrium dissociation constant ($K_D = K_d/K_a$), and goodness of fit (Chi square X^2 and R-square R^2). Kinetic constants were calculated in the case of a good fit ($X^2 < 3$ [$p > 0.05$] and $R^2 > 0.95$).

Liposome-flotation binding assay

SUVs of staphyloxanthin, PE and PG lipids were prepared as above, dispersed by sonication (1–2 min) and diluted in hydration buffer (1 mM final concentration). Flotillin variants (0.8 μg) were mixed with SUV and incubated (15 min, room temperature). The protein-lipid mixture was diluted 1:1 with 60% sucrose (w/v in 50 mM Tris-HCl pH 7.5, 200 mM NaCl) to form the bottom layer of the sucrose gradient (200 μL), which was overlaid with 250 μL 25% sucrose (w/v, same buffer) and a top layer of 100 μL buffer (0% sucrose). Samples were centrifuged (270,000 g, 1 h, 4°C). In a control experiment, we used Nile Red (0.1 mg/ml) to stain and localize lipids in the gradient; lipids localized in the top fraction. Top fractions were analyzed by immunoblot to detect flotillin variants.

Sucrose gradients

FloA oligomerization in *S. aureus* WT and Δcrt mutant and PBP2a oligomerization were analyzed in sucrose gradient assays. *S. aureus* cultures were harvested and cells crosslinked with 0.5 mM DSP (dithiobis(succinimidyl propionate)) before cell lysis and membrane fraction purification. Purified membrane fractions (200 μg) solubilized with 0.5% DDM were layered on a 5%–40% linear sucrose gradient generated by a Biocomp gradient maker, then centrifuged (Beckman; 100,000 g, 16 h, 4°C). Fractions (1 mL) were collected from the bottom of the gradient and proteins associated with each fraction were precipitated with 10% trichloroacetic acid (TCA). Protein fractions were dried and resuspended in PBS prior to immunoblot analyses.

Size exclusion chromatography

Purified WT flotillin and variants were adjusted to concentrations of ~ 60 μM and separated by size exclusion chromatography (Superose 6 increase 10/300 GL size-exclusion column; GE Healthcare) in an Äkta pure high-performance liquid chromatography (HPLC) system. For each size exclusion run, 500 μL protein sample was loaded onto a column equilibrated with buffer (300 mM NaCl, 50 mM Tris-HCl pH 8.0, 10% glycerol, 0.02% DDM) and run at a 0.4 mL/min constant flow rate. Protein elution profiles were compared by normalizing UV absorbance of the chromatograms and the graphs overlaid using PRISM. A set of standard proteins was used to calibrate the gel filtration column (Sigma-Aldrich MWGF1000-1KT).

Fluorescence microscopy

Cells from liquid cultures were washed in PBS and resuspended in 0.5 mL 4% paraformaldehyde (6 min, room temperature). Samples were washed twice and resuspended in 0.5 mL PBS. Images were acquired on a Leica DMI6000B microscope equipped with a CRT6000 illumination system, with a HCX PL APO oil immersion objective (100x1.47) and a color camera DFC630FX. Leica Application Suite Advanced Fluorescence Software was used for linear image processing. The YFP signal was detected (excitation filter 489 nm, emission filter 508 nm). Excitation times were 567 msec. Transmitted light images were taken with 55 msec excitation time.

Direct stochastic optical reconstruction microscopy

SNAP-tagged cells were incubated in SNAP buffer (250 mM Tris-HCl pH 7.5, 500 mM NaCl, 5 mM DTT (dithiothreitol)) and a final concentration of 0.8 μM SNAP-Cell TMR-Star dye (NEB; 30 min, 37°C in the dark). dSTORM was performed using an ELYRA S.1 super-resolution microscope (Zeiss) equipped with a 100x oil-immersion objective. Image stacks were analyzed with open source rapidSTORM software. Cluster analyses were performed by Python routine (Python 2.7.3, Python Software Foundation). Clusters were defined by one connected pixel area in image-based analysis or by a cloud of scattered localizations with spatial coherence, by calculating the standard deviation of the localization cloud from its center of mass.

Correlative light and electron microscopy

For high pressure freezing, overnight *S. aureus* cultures were pelleted and resuspended in 5% bovine serum albumin. Cell suspensions were pipetted into freezing plates (Leica Microsystems), cryoimmobilized, and processed. Briefly, cells were freeze-substituted, fixed with KMnO_4 and embedded in LR white resin (London Resin). Ultrathin 100-nm sections were mounted on glass slides and immunostained. For FloA labeling, we used polyclonal anti-FloA and Cy3-conjugated secondary antibody and for PBP2a, polyclonal anti-PBP2a (RayBiotech) and Cy5-conjugated secondary antibody. Detailed antibody information is found in the [Key](#)

Resources Table. For fluorescence microscopic analyses, we used the ELYRA S.1 super-resolution structured illumination microscope. For Scan-EM imaging, we used a field emission scanning electron microscope JSM-7500F (JEOL) with a LABE detector (for back-scattered electron imaging) at acceleration voltage 5 kV, probe current 0.3 nA, and a working distance of 6–8 mm. Image processing and correlation were as described (Markert et al., 2016).

Electron tomography

Samples were processed as for CLEM. High pressure frozen pellets were freeze-substituted, embedded, and processed (Helmprobst et al., 2015). Electron tomography was performed as described (Helmprobst et al., 2015) with modifications. Tilt series were acquired using an electron microscope JEM-2100 (JEOL) at 200 kV equipped with a F416 digital camera (TVIPS; 4096 × 4096 pixel resolution) automated with Serial EM software. Tilt angle ranges varied from $-65^{\circ}/65^{\circ}$ and $-70^{\circ}/70^{\circ}$. Tilt series were acquired systematically in 1° increments. For reconstruction of electron tomograms and segmentation, we used eTomo/IMOD.

Immunogold FloA detection

Fixed *S. aureus* cells were cryoimmobilized by rapid immersion in -170°C ethanol using Leica CPC equipment, and progressively cryosubstituted in -40°C methanol/0.5% uranyl acetate before embedding in Lowicryl HM20 resin and thin-sectioning (60 nm) with a Leica EM UC6 ultramicrotome. For immunogold labeling, grids were incubated with chicken anti-FloA antibody (1:10) and gold-conjugated rabbit anti-chicken antibody (BBI; gold particles 10 nm diameter, dilution 1:40). Samples were negatively stained with 2% uranyl acetate and lead citrate, and images acquired with a JEM 1011 transmission electron microscope (JEOL; 100 kV) and a Gatan Erlangshen ES1000W camera.

Lipid-protein complex analysis by electron microscopy

Staphyloxanthin, PE and PG SUV were dispersed in a sonication bath and diluted in reaction buffer (50 mM Tris-HCl pH 8, 200 mM NaCl). Purified FloA (0.6 μM , 0.001% DDM) was incubated alone or with 0.4 mM of each lipid sample (30 min, 37°C). The reaction mixture (5 μl) was applied to a copper grid before uranyl acetate staining and visualized using the JEM 1011 transmission electron microscope.

Label-free protein quantification by mass spectrometry

For sample preparation, proteins were reduced in 1x LDS sample buffer (Thermo Scientific) with 50 mM DTT (5 min, 95°C), alkylated with 120 mM iodoacetamide, precipitated with acetone and dissolved in 0.5% sodium deoxycholate (SDC; Sigma). Samples were digested with 0.5 μg LysC (Wako) and 0.5 μg trypsin (Promega). SDC was removed by ethyl acetate extraction, desalted with C18 stage tips, and dissolved in 2% acetonitrile.

NanoLC-MS/MS analyses were performed on an Orbitrap Fusion instrument equipped with an EASY-Spray ion source and coupled to an EASY-nLC 1000 (Thermo Scientific). Peptides were loaded on a trapping column (2 cm × 75 μm ID, PepMap C18, 3 μm particles, 100 \AA pore size) and separated on an EASY-Spray column (25 cm × 75 μm ID, PepMap C18, 2 μm particles, 100 \AA pore size) with a 120-min linear gradient from 3%–32% acetonitrile and 0.1% formic acid. MS scans were acquired in the Orbitrap analyzer at a resolution of 120,000 at m/z 200.

For data analysis, MS raw data file processing, database searches and quantification, we used MaxQuant. The search was performed against a *S. aureus* database derived from UniProt; a database containing common contaminants was also used. For protein quantitation, LFQ intensities were used. Proteins with less than two identified razor/unique peptides were dismissed. Further data analysis was done with in-house-developed R scripts. Missing LFQ intensities in control samples (total lysate) were imputed with values near the baseline.

Bacterial two-hybrid analysis

Bacterial two-hybrid analysis was used to quantify the interaction between FloA and PBP2a. The coding sequences were cloned into the bacterial two-hybrid expression vectors (EuroMedex) to generate N- and C-terminal fusions to the catalytic domains T25 and T18 of *Bordetella pertussis* adenylate cyclase. Pairwise combinations of plasmids were then cotransformed in *E. coli* BTH101 strain, which harbors a *lacZ* gene under the control of a cAMP-inducible promoter. After interaction, the T25 and T18 catalytic domains of the adenylate cyclase form an active enzyme, leading to cAMP production and hence to reporter expression. Plates were incubated (48 h, 30°C). pKT25-*zip* and pUT18C-*zip*, as well as pKT25 and pUT18C, served as positive and negative controls, respectively. For quantitative measurements, β -galactosidase levels were determined and results shown in Miller units.

Bacterial three-hybrid analysis

PBP2a and PBP2, RodA, PrsA, and FtsZ were cloned in pKNT25 and pUT18 vectors (Euromedex). A cotransformed strain was used for protein-protein interaction assays to determine PBP2a interaction efficiency with PBP2, RodA, PrsA, or FtsZ. These strains were subsequently transformed with pSEVA modulable plasmids (Silva-Rocha et al., 2013) that bear distinct replication origins and propagate in *E. coli* at low, medium, and high copy numbers (10 $\mu\text{g}/\text{ml}$ gentamicin) (Schneider et al., 2015). Experiments that required propagation of pSEVA vectors were performed in LB medium with 100 $\mu\text{g}/\text{ml}$ ampicillin and 10 $\mu\text{g}/\text{ml}$ gentamicin. For quantitative measurements, β -galactosidase levels were determined and results shown in Miller units.

Pull-down assay

Pull-down assays were performed in 1.5 mL reaction tubes and samples kept at 4°C throughout the experiment; 250–1000 μ L Ni-NTA resin (QIAGEN) was used in reactions. The volume needed depends on expression of the bait protein and must be determined empirically. Proteins were bound to resin (1 h, 4°C). To remove supernatant after each step, samples were centrifuged (1000 g, 2 min). To remove unbound and non-specific protein, the resin was washed twice with low-imidazole buffer. For elution, 100 μ L elution buffer was added twice; fractions were collected and protein content analyzed by LC-MS versus the eluted fraction of an unlabeled protein extract.

Blue-native PAGE

Cultures were grown in TSB medium (24 h, 200 rpm). Cells were harvested and the pellet dissolved in PBS buffer containing 1 mM PMSF and cOmplete protease inhibitors (Roche). Samples were crosslinked with 0.5 mM DSP before cell lysis and fractionation. The membrane fraction (\sim 80 μ g) was solubilized in 1x Native PAGE sample buffer (Invitrogen) with 0.5% DDM (overnight, 4°C). Solubilized membranes were mixed with Coomassie dye G-250 and loaded on a native gel with a 3%–12% polyacrylamide gradient (Invitrogen). BN-PAGE was carried out according to Wittig et al. (Wittig et al., 2006). BN-PAGE uses Coomassie G-250 to confer a negative charge to proteins and allows resolution of the oligomeric complexes according to their native state. Immunoblotting was used to detect FloA and PBP2a using specific polyclonal antibodies.

Western blot analysis and immunodetection

80 μ g total protein was separated in 12% SDS-PAGE. Proteins were transferred to a PVDF membrane by semi-dry blotting (2 h), which was blocked with 5% skim milk and human serum 2% (1 h) and probed with antibodies listed in Key Resources Table. Proteins were detected using a chemiluminescent substrate kit (Thermo Scientific) and recorded with the ImageQuant LAS4000 illumination system (General Electric).

Mouse infection studies

The *S. aureus* strains were cultured on BHI medium (18 h, 37°C). Cells were collected, washed three times with PBS and diluted to $OD_{600\text{ nm}} = 0.05$. Viable cell counts were determined by plating inoculum dilutions on TSB agar plates. For survival experiments, cohorts of 10 mice were infected with 150 μ L of *S. aureus* cultures (3×10^7 cells) via intravenous injection. Each strain was used to infect one mouse cohort. Doses of oxacillin (200 mg/kg) alone or in combination with ZA (50 mg/Kg or 20 mg/Kg) were injected intraperitoneally (i.p.) daily for 1–4 days. ZA concentration was chosen according to concentrations used in studies to evaluate statins as cholesterol-lowering agents in mice (Ghodke et al., 2012). The first dose was administered 30 min after the bacterial inoculation. Infections were allowed to progress until severe infection signs occurred or to a 3-day endpoint. Mice were sacrificed when they met the following criteria: 1) loss of at least 20% body weight, 2) loss of at least 15% body weight and ruffled fur, 3) loss of at least 10% body weight and hunched posture, or 4) 4 days post-infection. For bacterial load experiments, cohorts of 10 mice were instilled with *S. aureus* suspension (3×10^8 cells) into left nare of anesthetized mice. Doses of oxacillin (200 mg/kg) alone or combined with ZA (50 mg/Kg or 20 mg/Kg) were injected i.p. daily for 1–2 days. The first dose was administered 30 min after bacterial inoculation. Infection was allowed to progress for two days. Mice were sacrificed and lungs collected aseptically, homogenized in 2 mL sterile PBS in GentleMACS M Tubes (Miltenyi Biotec); serial dilutions were plated on mannitol-agar plates and incubated (24 h, 37°C).

Software used in this study

Protein MS data were analyzed with MaxQuant (<http://www.coxdocs.org/doku.php?id=maxquant:start>) and deposited in ProteomeXchange via the Pride Partner repository (<https://www.ebi.ac.uk/pride/archive>). For lipidomics assays, we used MassLynx (http://www.waters.com/waters/en_US/MassLynx-Mass-Spectrometry-Software-/nav.htm?cid=513164&locale=en_US). Data were analyzed with Progenesis software (<http://www.nonlinear.com/progenesis/qj>). To quantify the fluorescent signal in fluorescence microscopy images, we used the LAS Leica Application Suite (<http://www.leica-microsystems.com/products/microscope-software>); for processing, modeling, and display programs for tomographic and 3D reconstruction of EM serial sections, we used IMOD software (<http://bio3d.colorado.edu/imod>).

QUANTIFICATION AND STATISTICAL ANALYSIS

Statistical analyses

All statistical analyses were performed using Sigma-Plot software (Systac Software). Graphs represent data from at least three independent biological replicates. Each biological replicate represents three independent technical replicates ($n = 3$). Data are shown as mean \pm SEM. For analysis of experiments with two groups, we used the parametric unpaired two-tailed Student's *t* test with Welch's correction and the non-parametric unpaired Mann-Whitney test. For analysis of experiments with three or more groups, the parametric one-way ANOVA test was used. *Post hoc* analysis included multiple comparisons Tukey's test, Dunnett's test or

Dunn's tests, depending on the dataset. Differences were considered significant when p was < 0.05 . ns = not significant, * $p < 0.05$, ** $p < 0.01$, *** $p < 0.001$.

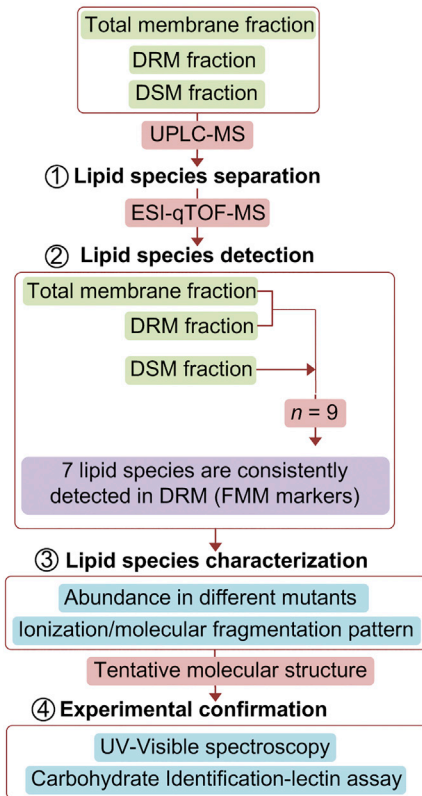
DATA AND SOFTWARE AVAILABILITY

Data availability

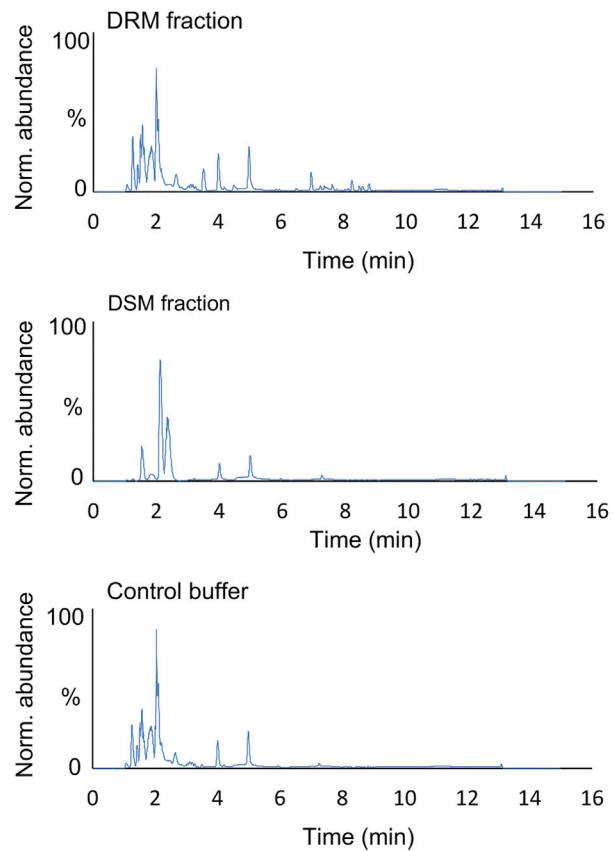
Original unprocessed images (gels and western blots, microscopy images and movies) have been deposited in Mendeley data (<https://data.mendeley.com/>) under the Reserved DOI: <https://doi.org/10.17632/zr92hyx6y5.1>.

The mass spectrometry proteomics have been deposited at the ProteomeXchange Consortium via the Pride Partner Repository, with the dataset identifier PRIDE: PDX00654C.

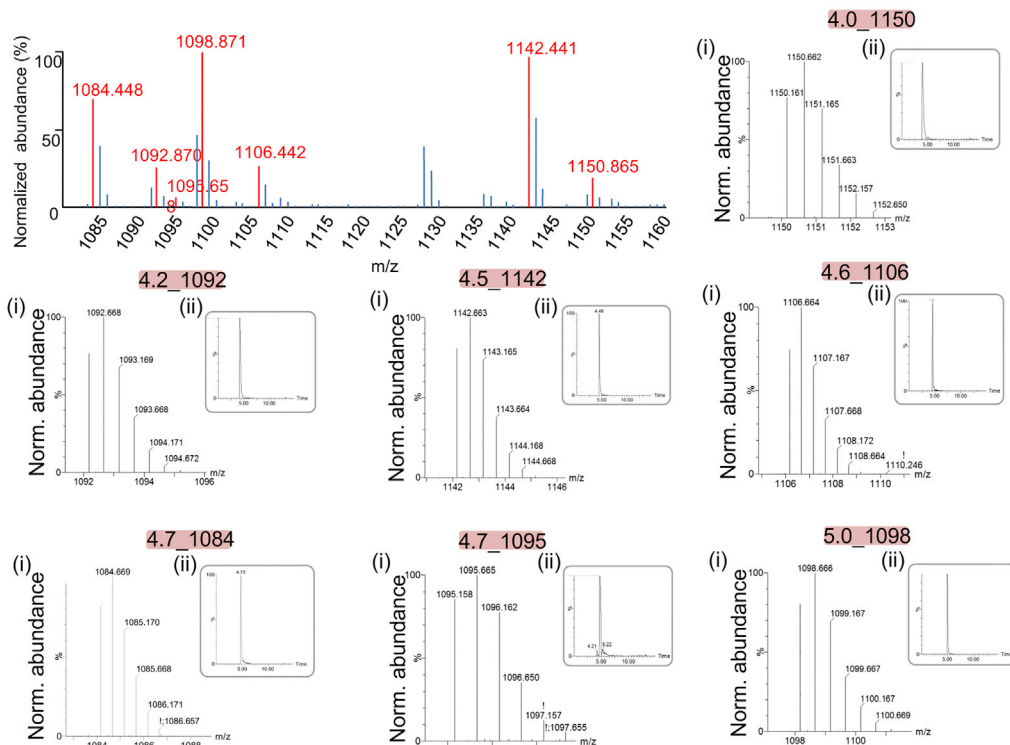
A



B



C



(legend on next page)

Figure S1. Detection of FMM Lipid Markers in the DRM Fraction, Related to Figure 1

(A) Scheme of the workflow to identify the most abundant DRM lipid markers using ultra-performance liquid chromatography coupled to mass spectrometry equipped with electrospray ionization source (UPLC-ESI-qTOF-MS). DRM lipid composition was compared to the control sample (buffer only). Of 2044 peaks, 39 were detected exclusively in the DRM fraction. The abundance of these peaks was determined in DSM samples; of the 39 peaks detected, 30 were not detected in the DSM fraction and were thus exclusive to the DRM fraction. Data for three independent biological replicates ($n = 3$) showed a consistently high concentration of 7 of the 30 peaks in the DRM versus DSM fraction. Univariate statistical analysis (using three filters; infinite in FMM-enriched sample, signal-to-noise ratio of the most abundant peak > 50 [area in progenesis: 10,000], and correlation variance $< 10\%$). These peaks were thus considered lipid markers for FMM. Detection of the peaks in different mutants and examination of the molecular fractionation pattern generated a tentative molecular formula. Experimental confirmation of the most significant features associated with the tentative molecular formula were confirmed by UV spectroscopy (to confirm that the molecule is a staphyloxanthin derivative) and lectin-probed sugar identification assay (to confirm that the molecule bears diverse sugars such as N-acetylglucosamine and N-acetylmuramic acid).

(B) Total ion chromatograms of lipid species in the DRM fraction (top), DSM fraction (center) and buffer control (bottom) using UPLC-ESI-qTOF-MS.

(C) Top, MS spectrum of the DRM fraction. The 7 FMM lipid markers are highlighted with their m/z values. Bottom, ionization and retention behavior of the 7 FMM lipid markers. MS spectra using negative ESI (i) and extracted chromatogram (ii) of the 7 FMM lipid markers. In (i), the y axis represents normalized abundance and the x axis, mass-to-charge ratio (m/z). In (ii), the y axis shows normalized abundance and the x axis, retention time (RT). Marker features were annotated as 4.0_1150, 4.2_1092, 4.5_1142, 4.6_1106, 4.7_1084, 4.7_1095, and 5.0_1098, according to their RT and nominal m/z . An RT between 4-5 min suggests polar characteristics of the markers (phospholipids elute at 6-8 min, triacylglycerols at 8-10 min). Mass spectra indicated a double-charged ion, since the mass difference of isotope peaks were 0.496-0.503 Da and the most abundant isotope was the second peak in all profiles.

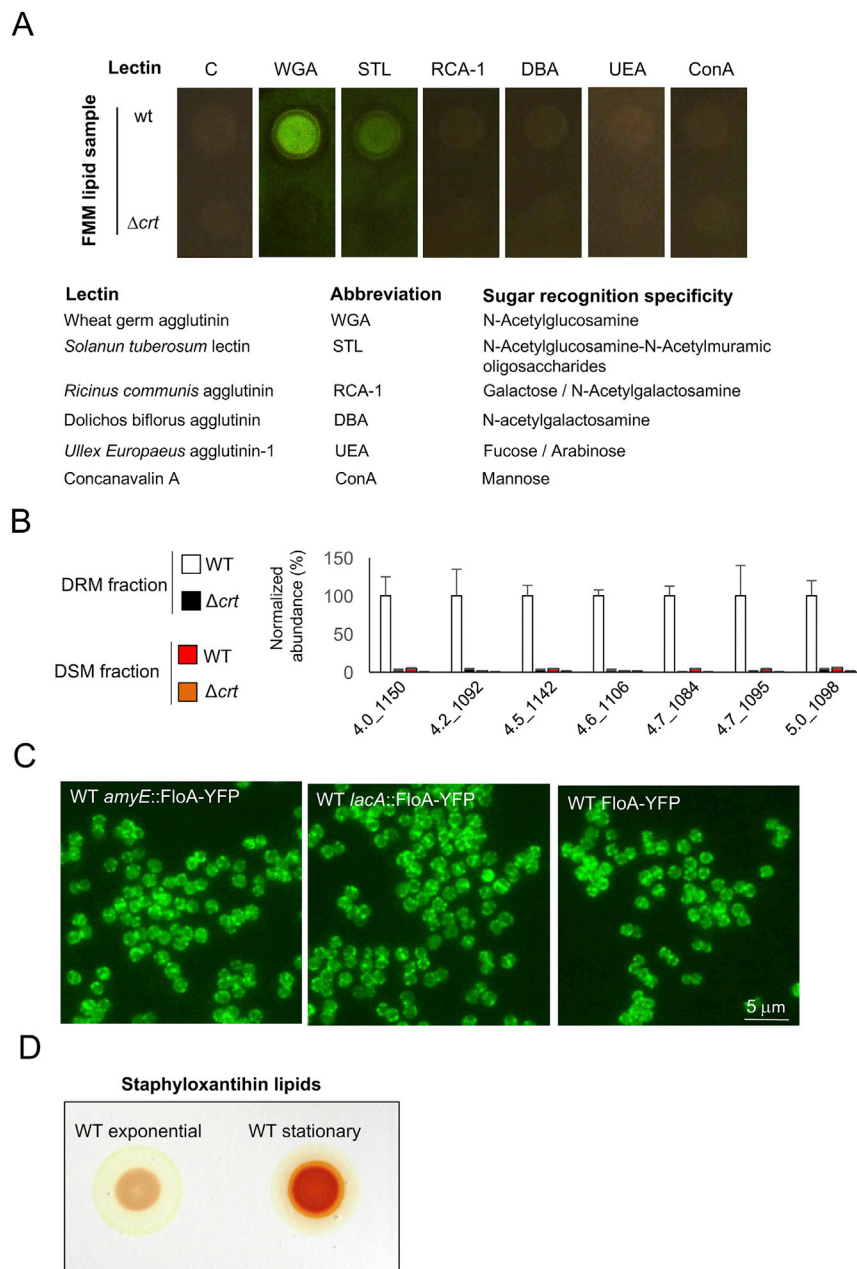


Figure S2. Identification of FMM Lipid Markers, Related to Figures 1 and 2

(A) Lectin-probed blot analyses of FMM lipid samples from *S. aureus* wild-type (WT) and the staphyloxanthin-deficient strain (Δcrt mutant). Carbohydrates bound to the FMM lipids were identified based on the specific carbohydrate-binding properties of various lectins used in this assay. FMM lipids from WT and the Δcrt mutant were purified and immobilized on TLC membranes, which were blocked (10% non-fat milk) and incubated with distinct fluorescein-labeled lectins. After washing, a fluorescence signal is detected only if lectins are bound to the FMM lipids, through recognition of the sugars borne by the lipids. The lectins used and their recognition specificities are shown in the figure. Control sample (C) was incubated with no lectin, to detect sample autofluorescence. Positive signal was obtained with WGA and STL lectins in the WT sample but not the Δcrt mutant.

(B) Quantitative determination of FMM lipid markers in DSM and DRM fractions in WT and Δcrt using UPLC-ESI-qTOF-MS. The y axis shows normalized abundance; FMM lipid markers in the x axis are named according to RT and m/z (RT_m/z). FMM lipid markers were concentrated in the DRM fraction, and were not detected in Δcrt fractions. Data shown as mean \pm SD of three independent biological replicates.

(C) Fluorescence micrographs of MRSA cells expressing FloA-YFP at different integration sites in the chromosome. Bar, 5 μ m.

(D) Purification of staphyloxanthin lipids from exponential and stationary MRSA cultures. Samples were spotted on a TLC plate. Staphyloxanthin lipids are produced in cultures in exponential and stationary phases.

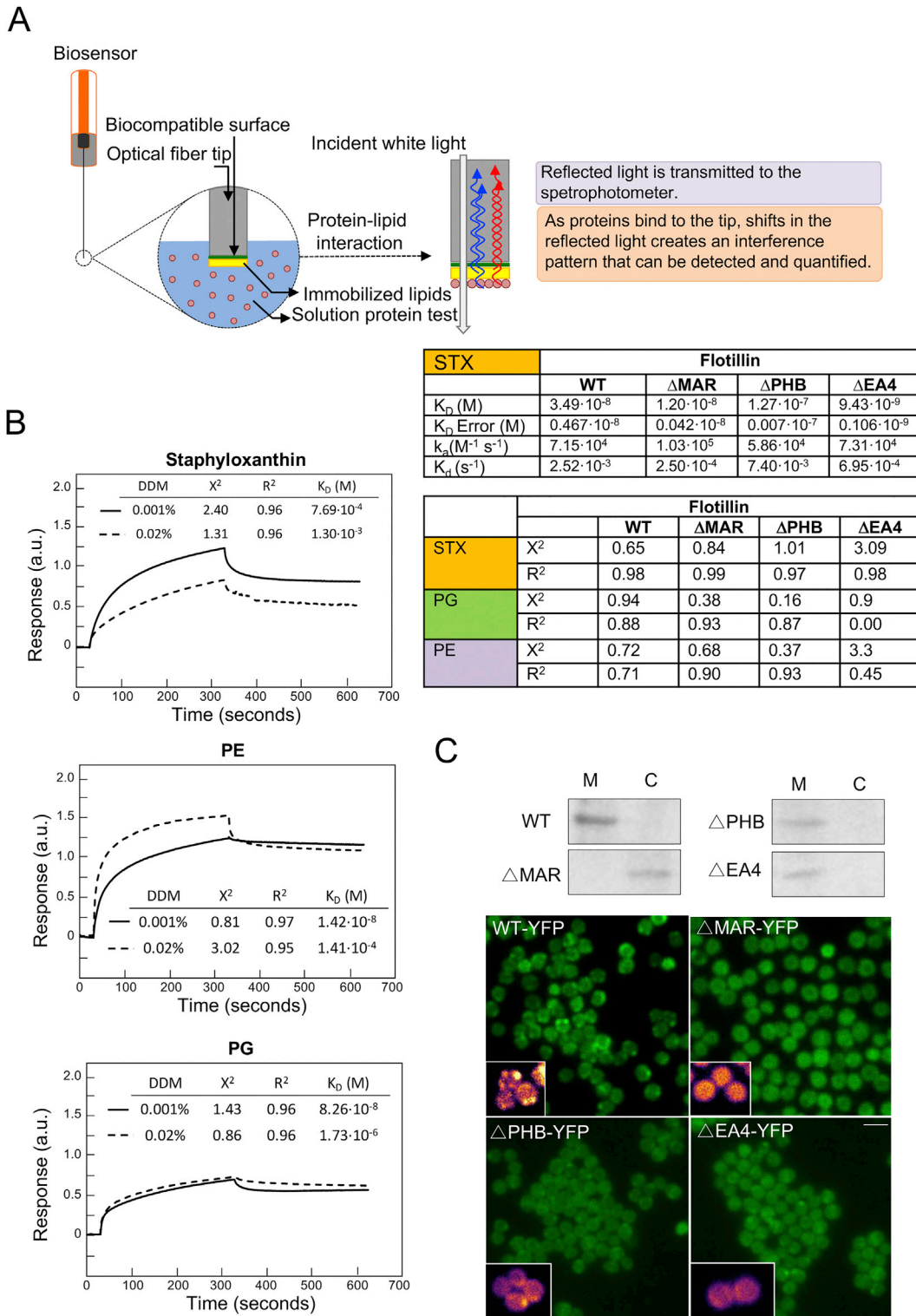


Figure S3. Flotillin Preferentially Binds Staphyloxanthin, Related to Figure 2

(A) Top, bio-layer interferometry (BLI) to assay lipid-protein interactions. This optical-analytical technique monitors the interference pattern of white light reflected from two surfaces, a layer of immobilized lipids on the biosensor tip, and an internal biocompatible surface (left). Any change in the number of proteins bound to the biosensor tip causes a shift in the interference pattern that can be detected and quantified (right). Interactions are measured in real time, providing the ability to monitor binding specificity with association/dissociation rates. Bottom, interaction between staphyloxanthin and the FloA variants (WT, Δ MAR, Δ PHB, Δ EA4)

(legend continued on next page)

were measured using BLI. Purified staphyloxanthin was immobilized on aminopropylsilane biosensor tips. 0.5 μM protein solution was added and affinity constants (K_D) calculated using K_a (association) and K_d (dissociation) rate constants. Values are the mean of three independent experiments. Chi-square χ^2 and R^2 indicates goodness of fit. As control, interaction of flotillin variants with membrane phosphatidylethanolamine (PE) or phosphatidylglycerol (PG) was tested. The signal in these control assays did not fit association and dissociation kinetics thus their χ^2 and R^2 showed poor fit and affinity constants K_D could not be extracted.

(B) Control experiments using BLI showing staphyloxanthin, PE or PG binding to the biosensor tip. These experiments tested two dissociation conditions with buffer containing 0.001% (solid line) or 0.02% (dashed line) DDM (docecylmatoside); 0.001% is the DDM concentration used to test FloA binding to lipids in BLI experiments (main Figure 2E). Conditions using 0.02% DDM were 20-fold higher DDM concentration than normal resting conditions. Affinity constants (K_D) and goodness of fit χ^2 and R^2 were calculated for both binding conditions. Values are the mean of three independent experiments. In both cases, lipid binding fit an association curve correctly, showing marked, predictable, and reproducible staphyloxanthin and PE or PG association to the biosensor. The presence of DDM in the buffer at the concentrations used to test flotillin binding or higher did not cause marked lipid dissociation from the biosensor tip. Response measured in arbitrary units (a.u.).

(C) Top, immunodetection of FloA-YFP (WT) and YFP-labeled flotillin variants (ΔMAR , ΔPHB , ΔEA4) in *S. aureus* cytoplasmic and membrane fractions, using polyclonal anti-YFP antibodies. Bottom, fluorescence microscopy analyses of subcellular localization of FloA-YFP (WT) and YFP-labeled flotillin variants (as above) in *S. aureus* cells. Bar, 5 μm .

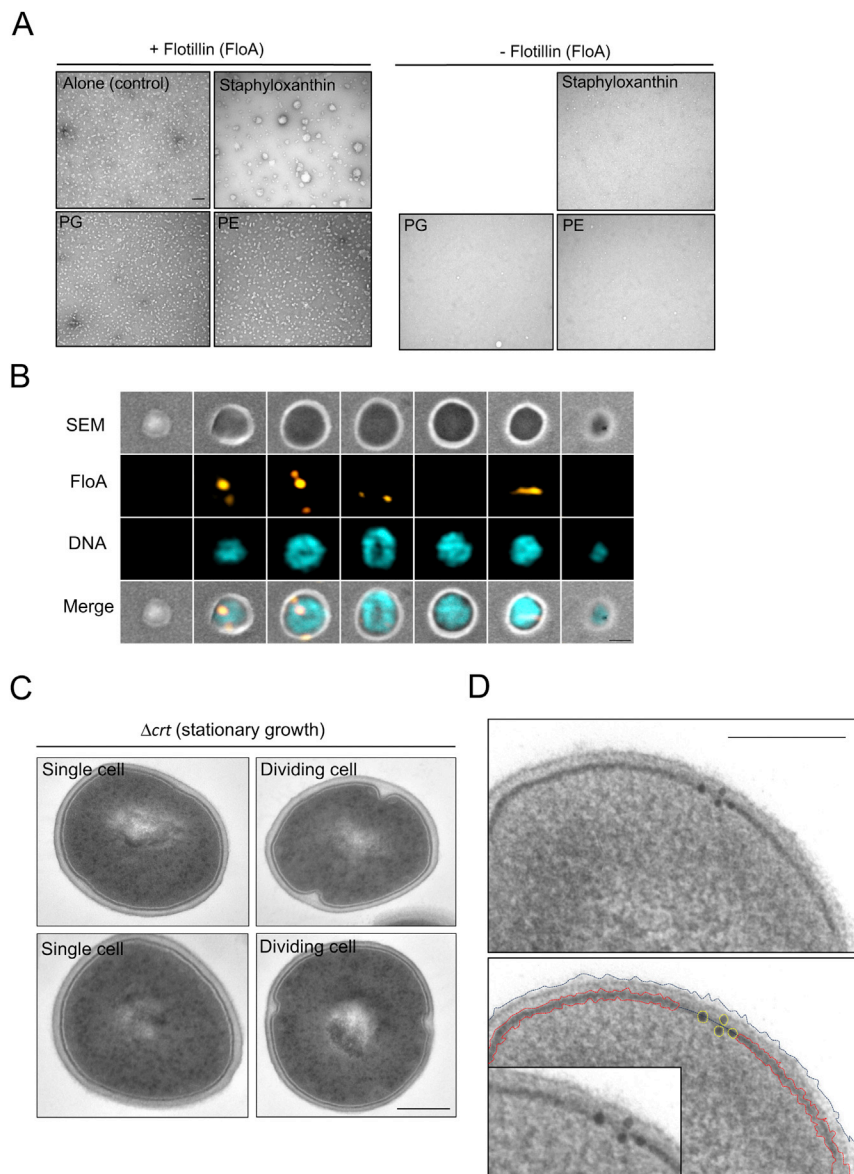


Figure S4. Visualization of FMM in Whole Cells, Related to Figures 3 and 4

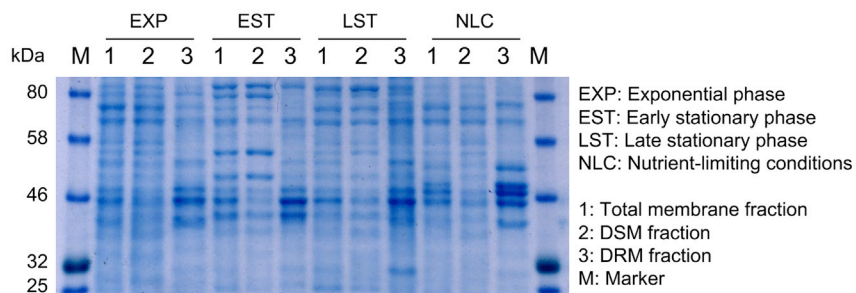
(A) Left, TEM micrographs of purified flotillin oligomers alone or preincubated with staphyloxanthin or PE/PG. Staphyloxanthin-incubated FloA oligomers generated larger protein assemblies. Fields corresponding to detailed micrographs (Figure 3C). Right, control TEM micrographs of purified lipids alone (staphyloxanthin or PE/PG). In the absence of flotillin, lipid samples do not organize large assemblies. Bar, 100 nm.

(B) Super-resolution array tomography (srAT) using structural illumination microscopy (SIM) and scanning electron microscopy (Scan-EM) (SIM +Scan-EM) of *S. aureus* cells. Cells are embedded in a methacrylate matrix and thin-sectioned in 100-nm slices. Columns show each of the 100-nm sections from an entire cell. FloA was immunodetected with Alexa 488-conjugated secondary antibody (yellow signal, second row). DNA was stained using Hoechst 33258 dye (blue signal, third row) to determine cell contour in fluorescence microscopy images. The Scan-EM image is used as background (first row). First right column shows a merge of all three channels. Bar, 1 μ m.

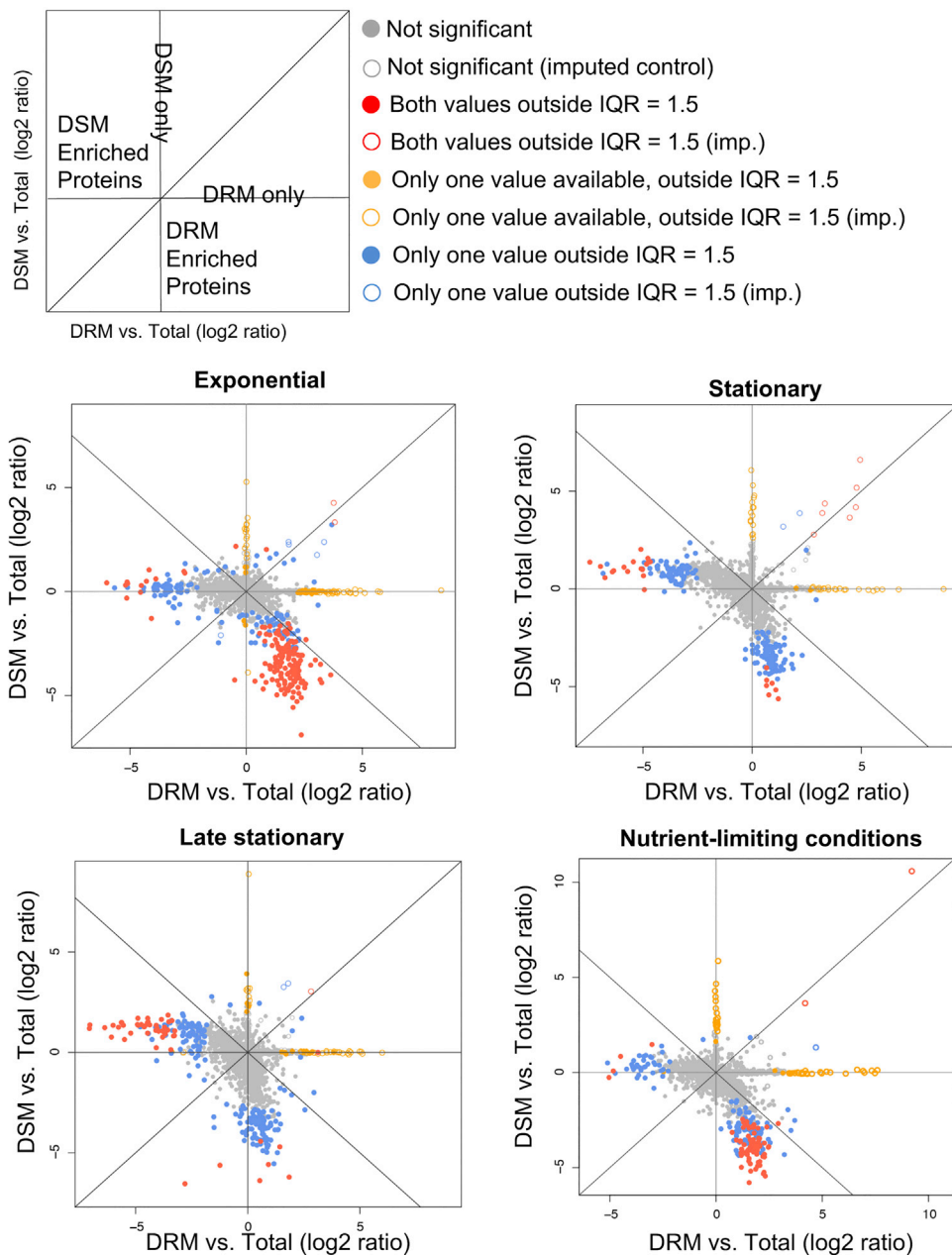
(C) Control TEM micrographs of staphyloxanthin-deficient cells (Δcrt mutant) collected at stationary phase. Left, single cells; right, dividing cells. Uranyl acetate staining shows cell membranes with more uniform electron contrast in the Δcrt mutant than WT cells. Bar, 300 nm.

(D) Top, immunogold labeling of FloA in thin-sectioned cells visualized by TEM. Gold particles (10-nm diameter) localized in discrete membrane foci. FloA signal colocalizes with light electron-dense membrane areas. Bottom, differential electron density map of FloA immunogold-labeled TEM image. Gold particles labeled in yellow. This map corresponds to the image in Figure 4C. Bar, 300 nm.

A



B



(legend on next page)

Figure S5. Identification of Proteins Localized Preferentially in DRM Fractions Using LFQ, Related to Figure 6

(A) SDS-PAGE analysis of DRM and DSM fractions, which show comparable protein concentrations in the four growth conditions tested (exponential phase, EXP; early stationary phase, ESP; late stationary phase, LST, and nutrient-limiting conditions, NLC). *Staphylococcus aureus* was grown in TSB medium (37°C, 200 rpm). For EXP, cells were collected after 3 h incubation, for ESP, after 12 h and for LST, after 24 h. For NLC, cells were grown in TSB medium supplemented with 0.5 mM dipyriddy (12 h, 37°C, 200 rpm).

(B) Protein quantification using label-free liquid chromatography-mass spectrometry (LC-MS). Scatterblots of identified proteins are given as normalized log₂ ratios. Each dot represents one protein. After normalization, DRM versus total membrane ratio was plotted (y axis) and DSM versus total membrane (x axis) for each growth condition. Imputed values (Imp.) indicate that, for log-ratio calculation, protein detected in DRM or DSM was not detected in the “total membrane fraction.” This could be due to sample complexity, which renders some proteins below our detection limit. Although the value for these proteins would be 0, we used an imputed value of 1 to enable ratio calculation. These proteins are indicated by unfilled colored circles. Colored dots are proteins outside an interquartile range (IQR) of 1.5. IQR is a measure of statistical dispersion of the data, as it determines the difference between upper and lower quartiles. Statistically significant outliers (outside the IQR; these proteins show enrichment in one fraction versus the other) are colored dots. Non-significantly enriched proteins are shown in gray. Red dots are proteins whose DRM and DSM measurements are both outside IQR = 1.5; blue dots are those with only one value outside IQR = 1.5 and for yellow dots, only one value was available (proteins detected exclusively in DRM or DSM). The scheme shows various scatterblot zones representing proteins found exclusively or enriched in DSM or DRM.

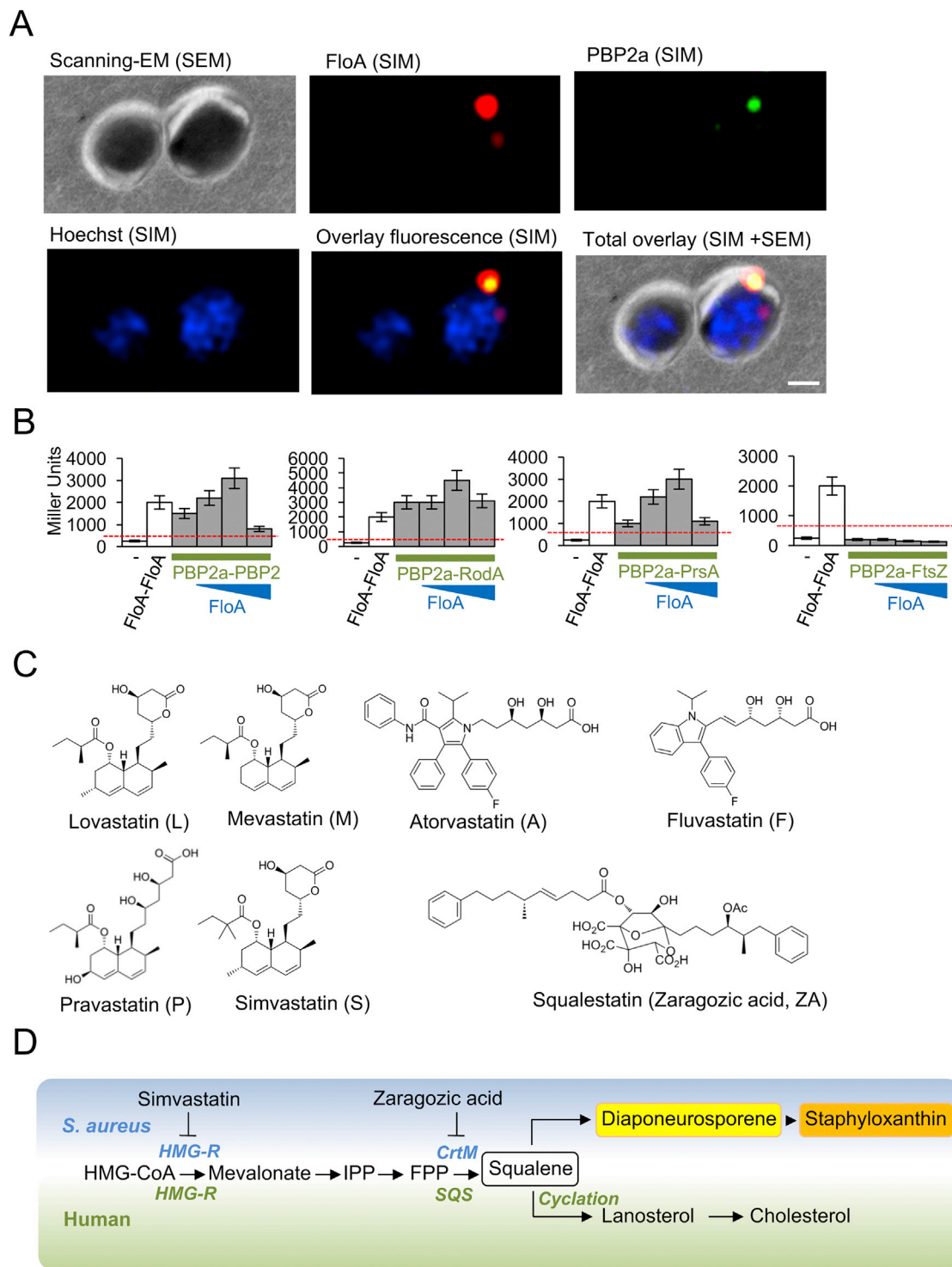


Figure S6. Flotillin Scaffold Activity Contributes to PBP2a Oligomerization, Related to Figure 7

(A) SrAT (SIM+Scan-EM) 100-nm thin section image of *S. aureus* cells. For FloA immunodetection, Cy3-conjugated secondary antibody was used (red) and for PBP2a, Cy5-secondary antibody (green). DNA was Hoechst 33258-stained (blue). Overlay shows the merge of all signals. PBP2a and FloA signals colocalized in discrete membrane foci. Bar, 300 nm.

(B) Bacterial three-hybrid analysis showing interaction of PBP2a with the tentative interacting partners PBP2, PrsA and RodA, and the non-interacting control protein FtsZ at distinct FloA concentrations. Three pSEVA plasmids were used to express FloA at distinct concentrations. pSEVA 621, 631 and 641 plasmids maintain similar backbones and expressed *floA* under the control of a constitutive promoter. Plasmids bear different replication origins; pSEVA 621 carries the

(legend continued on next page)

low-copy-number replication origin RK2, pSEVA 631, the medium-copy-number replication origin pBR1, and pSEVA 641, the high-copy-number replication origin pRO1600. The strains carrying each of these plasmids thus produce FloA at different concentrations as a direct function of the *floA* copy number expressed. Dashed red line indicates the threshold limit that defines a positive (≥ 700 Miller units) or negative interaction signal (< 700 Miller units). Data shown as mean \pm SD of three independent biological replicates.

(C) Molecular structure of the statins tested in this study.

(D) Scheme of the mevalonate pathway and its bifurcation to produce staphyloxanthin-related lipids in *S. aureus* (blue background) or cholesterol in humans (green). Zaragozic acid (ZA) is a competitive inhibitor in both routes, acting downstream of formation of farnesyl pyrophosphate (FPP). Statins such as simvastatin also inhibit both routes, as they inhibit the enzyme HMG-CoA reductase.

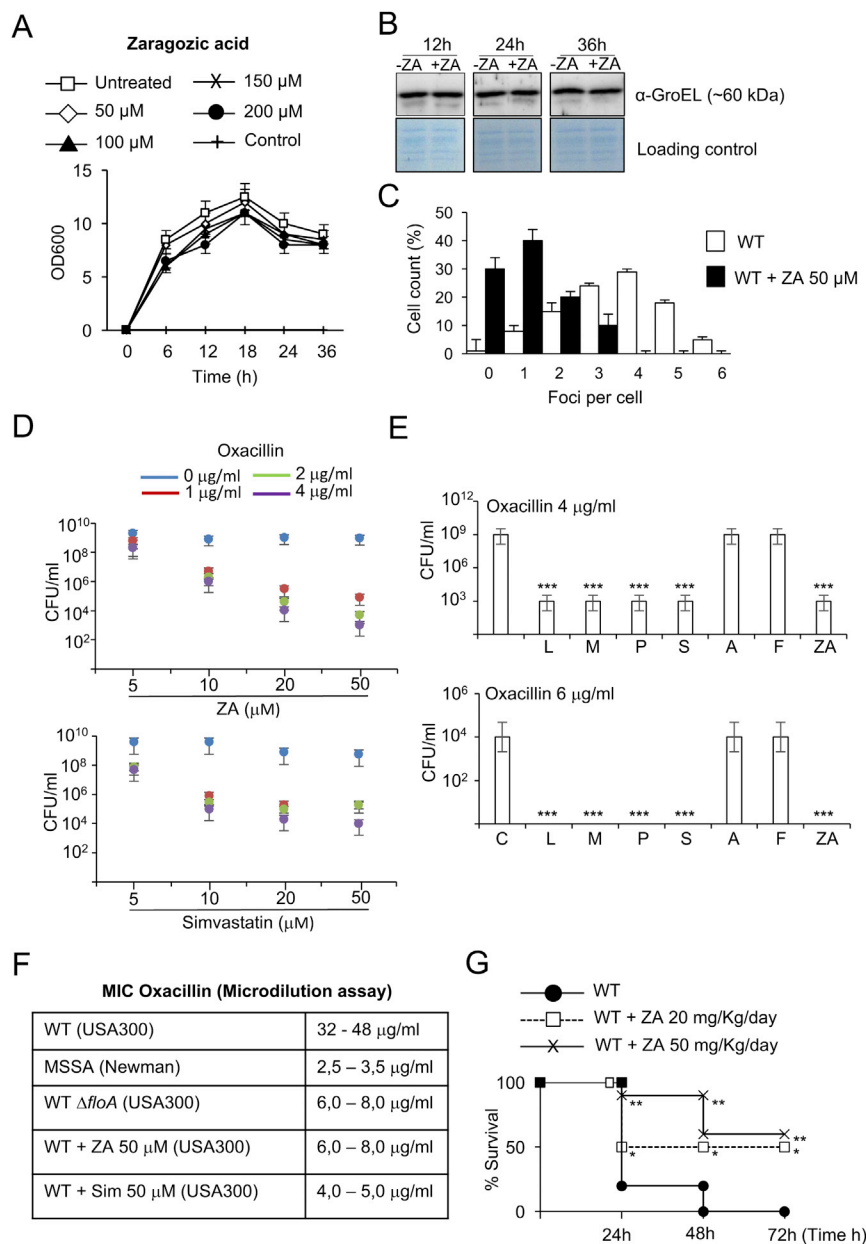


Figure S7. Synergistic Antimicrobial Effect of Statin and β -Lactam Antibiotics, Related to Figure 7

(A) Growth curves of *S. aureus* cultures at different ZA concentrations. Cultures were grown in TSB medium and incubated (36 h, 37°C, 200 rpm). ZA addition to cultures did not affect *S. aureus* growth at the concentration used (50 μ M). Data shown as mean \pm SD of three independent biological replicates.

(B) Immunodetection of the chaperonin GroEL in *S. aureus* cell extracts. Untreated (control) and treated samples (ZA) showed comparable GroEL levels, suggesting that *S. aureus* treatment with ZA at the concentration tested had no pronounced effects on major cell processes or weakened cell physiology.

(C) Measure of the reduction in focus number in ZA-treated *S. aureus* cells. We counted 700 random cells from each of three independent microscopic fields in independent experiments ($n = 2100$ cells total/strain).

(D) Bacterial count (colony-forming units/ml) of MRSA cultures treated with a combination of ZA or simvastatin and the β -lactam antibiotic oxacillin. MRSA growth was unaltered in the presence of ZA or simvastatin. Growth was inhibited by oxacillin if ZA or simvastatin were added to the cultures. Increasing ZA or simvastatin concentration in the cultures potentiated the antibiotic effect of oxacillin.

(E) Bacterial count (CFU/ml) of MRSA cultures treated with a combination of statins and the β -lactam antibiotic oxacillin. L, lovastatin; M, mevastatin; P, pravastatin; S, simvastatin; A, atorvastatin; F, fluvastatin, ZA, zaragozic acid. Whereas some statins inhibited growth in response to oxacillin, others such as atorvastatin or fluvastatin did not alter the MRSA antibiotic-resistant phenotype. We attribute this "all-or-nothing" effect to the properties of certain molecules, which prevents their penetration of the cell envelope and thus, encounter with the target (the cytoplasmic enzyme CrtM). Data shown as mean \pm SD of three independent biological replicates. Statistical analysis was carried out using an unpaired Student's *t* test (** $p < 0.001$).

(legend continued on next page)

(F) Oxacillin minimal inhibitory concentration (MIC) antibiotic susceptibility test of different strains (MRSA and MSSA strains), mutants (the $\Delta floA$ MRSA mutant) and ZA- or simvastatin-treated MRSA strains.

(G) Survival curve of oxacillin-treated mice infected with ZA-treated WT (3×10^7 cells; $n = 10$). ZA was administered at two concentrations. Statistical analysis, one-way ANOVA with Tukey's comparison between WT versus WT+ZA (* $p < 0.05$, ** $p < 0.01$).